Review

Confinement Effects in Well-Defined Metal–Organic Frameworks (MOFs) for Selective CO_2 Hydrogenation: A Review

Xiaofei Lu [1,2], Chuqiao Song [1], Xingyu Qi [2], Duanxing Li [2] and Lili Lin [1,*]

1   Institute of Industrial Catalysis, State Key Laboratory of Green Chemistry Synthesis Technology, College of Chemical Engineering, Zhejiang University of Technology, Hangzhou 310014, China
2   Department of Chemical System Engineering, School of Engineering, The University of Tokyo, Tokyo 113-8656, Japan
*   Correspondence: linll@zjut.edu.cn

Abstract: Decarbonization has become an urgent affair to restrain global warming. CO_2 hydrogenation coupled with H_2 derived from water electrolysis is considered a promising route to mitigate the negative impact of carbon emission and also promote the application of hydrogen. It is of great significance to develop catalysts with excellent performance and large-scale implementation. In the past decades, metal–organic frameworks (MOFs) have been widely involved in the rational design of catalysts for CO_2 hydrogenation due to their high surface areas, tunable porosities, well-ordered pore structures, and diversities in metals and functional groups. Confinement effects in MOFs or MOF-derived materials have been reported to promote the stability of CO_2 hydrogenation catalysts, such as molecular complexes of immobilization effect, active sites in size effect, stabilization in the encapsulation effect, and electron transfer and interfacial catalysis in the synergistic effect. This review attempts to summarize the progress of MOF-based CO_2 hydrogenation catalysts up to now, and demonstrate the synthetic strategies, unique features, and enhancement mechanisms compared with traditionally supported catalysts. Great emphasis will be placed on various confinement effects in CO_2 hydrogenation. The challenges and opportunities in precise design, synthesis, and applications of MOF-confined catalysis for CO_2 hydrogenation are also summarized.

Keywords: metal–organic frameworks; MOF-derived materials; confinement effects; selective CO_2 hydrogenation; immobilization; encapsulation; size effect; synergy effect; interface catalysis

1. Introduction

Valorization of CO_2 is a prerequisite for achieving a "carbon-neutral society" as declared in the 2015 Paris Agreement. The chemical conversion of CO_2 into value-added and energy-intensive chemicals is a promising approach to achieve this goal, especially when driven with the green hydrogen from water electrolysis powered by renewable electricity. Accordingly, intensive research efforts have been dedicated to selective CO_2 hydrogenation to CO, formic acid, hydrocarbons, or oxygenates [1–5]. However, these processes suffer from slow kinetics and low selectivity due to the strong strength of the C=O double bond (806 kJ mol^{-1}) [6]. Many advances have been made in various heterogeneous CO_2 hydrogenation catalysts, including oxide (e.g., $Cu/ZnO/Al_2O_3$ and $ZnO-ZrO_2$), oxide/zeolite (e.g., $Na–Fe_3O_4/HZSM-5$ and $ZnZrO_x/SAPO-34$), supported monometallic or bimetallic catalysts (Ru, Ir, Pt, Rh, PtCo, and PdRh), and immobilized molecular complexes [7–23]. The active sites are carefully designed to process special structural and electronic properties for desired products. For example, the inverse ZrO_2/Cu was designed to maximize the $Cu-ZrO_2$ interface, which promoted CH_3OH synthesis activity and selectivity of supported Cu [24]. The 8 nmsized Ni supported on CeO_2 exhibited superior CH_4 selectivity over the 4 nm and 2 nm counterparts in CO_2 hydrogenation due to the structure and size dependency [25]. The artificial (C_{2+}) hydrocarbons or their oxygenated derivatives could

be produced via the rational design of catalysts using zeolite [26,27]. Hence, the rational design of efficient catalysts is essential for achieving high catalytic activity and selectivity during CO_2 hydrogenation [28,29].

Besides the rational design of efficient catalysts, the confinement effects are also widely utilized to stabilize active sites during catalytic CO_2 hydrogenation [21,30–32]. The strong interactions between metal nanoparticles (NPs) and supports (e.g., $Cu/\beta\text{-}Mo_2C$, Ir/CeO_2, $Ni/\gamma\text{-}Mo_2N$) are confirmed as an effective confinement strategy to prevent the aggregation of NPs [33–35]. It modifies the electronic and geometric structures of catalytic active sites. However, the catalyst structure derived from the strong metal–support interaction (SMSI) effect is limited to certain metal and support combinations. Encapsulating the NPs with porous materials or membranes (e.g., zeolite), and thus increasing their resistance to sintering, is another effective and versatile strategy [36–39]. The fixation of metal NPs with diameters of 0.8–3.6 nm into zeolite crystals (NPs@zeolite) was demonstrated to be sinter-resistant at 600–700 °C and outperformed conventionally supported metal catalysts (NPs/zeolite) during CO_2 hydrogenation [36,37,40]. Unlike the utilization of SMSI or the encapsulation by the zeolite (with fixed tetrahedral Si/Al coordination and pore sizes <1 nm), the ordered three-dimensional metal–organic frameworks (MOFs), with uniform cavities, tunable local environments, tailorable composites, and versatility to introduce functional coordinators/groups, are highly attractive for the rational design of heterogeneous catalysis with confinement effects.

The last decades have witnessed intensive research efforts in the reticular design of various MOFs (>100,000), which have been explored in gas storage and separation, vapor sorption, catalysis, biomedical application, and chemical sensing [41,42]. This review only focuses on CO_2 hydrogenation, where the high surface area and porosity of MOFs are composed of various organic linkers, which can strongly bind metal atoms/clusters to serve as active sites, proffering the ability to adjust the structural and electronic modularity [5,43,44]. These composite materials can combine both the confinement effect of the pores and the SMSI or synergistic effects between active sites and organic chelates/metal-oxo clusters, providing new opportunities in finely tuning the performance of CO_2 hydrogenation [45–47]. Tsung and coworkers successfully encapsulated atomic sites or ultra-small NPs in MOFs via a post-synthesis method, which exhibited good activity and selectivity for CO_2 hydrogenation to formic acid, CH_3OH, and C_2H_5OH, respectively [48–52]. Moreover, metal or metal oxide NPs embedded in a porous carbon matrix can be produced by the pyrolysis of MOFs. Since various elements in MOFs are initially well ordered, the new structures can also contain highly dispersed single atoms, metal NPs, alloys, or dopants (e.g., N, P, S, or B) (in the case of dopant-containing organic linkers) [53–55]. Compared with conventional catalysts, the metal species are partially encapsulated by the deposited carbon, which exhibits enhanced thermal stability in high-temperature CO_2 hydrogenation reaction conditions. For instance, iron (Fe)- and cobalt (Co)-containing nanomaterials derived from MOFs showed superior selectivity and stability for CO_2 hydrogenation compared with traditional metal catalysts [56–58]. These pieces of evidence indicate that the introduction of well-defined MOFs or MOF-derived materials with identical coordinated environments is an effective strategy to unravel the key active sites for CO_2 hydrogenation catalysts, and then enhance the catalytic activity and selectivity.

In recent years, several reviews have introduced advances in the synthesis, characterization, and application of zeolite-fixed metal NPs as metal@zeolite catalysts [8,37,39,59]. For example, Xiao and coworkers reviewed the reported strategies for the construction of metal@zeolite hybrid materials and described how the zeolite micropore and metal nanoparticle synergistically worked to improve the catalytic performance [37,39]. Janiak and coworkers highlighted the confinement of noble nanometals in a zeolite matrix in heterogeneous catalysis [59]. Li et al. summarized the development of MOFs encapsulating active nanoparticles as emerging composites for various catalysis, including thermal catalysis, electrocatalysis, and photocatalysis [60,61]. These works all produced excellent reviews on the preparation of porous materials–confined metals and their applications

in heterogeneous catalysis. However, a comprehensive review on confined catalysis in MOFs or MOF-derived materials for CO_2 hydrogenation is still lacking. The current review mainly focuses on the confinement effects in MOFs or MOF-derived materials during CO_2 hydrogenation, as shown in Figure 1. Beginning with the introduction of the preparation and application of MOF-confined catalysts, the confinement effects on CO_2 hydrogenation will be discussed including molecular complexes in the immobilization effect, atomic sites in the size effect, cage stabilization in the encapsulation effect, and adsorption and activation in the synergy effect. Furthermore, the product distribution perturbed by MOF-derived materials during CO_2 hydrogenation will be interpreted. Finally, an outlook on the future development of MOF-based confined catalysis for CO_2 hydrogenation will be given. We hope that the mechanistic insights interpreted by confinement effects in MOFs or MOF-derived catalysts for CO_2 hydrogenation could facilitate the development of clear structure–activity relationships for rational catalyst design.
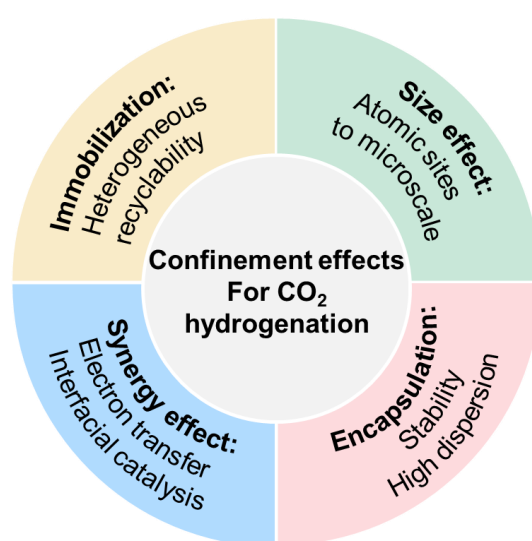

Figure 1. The summary of confinement effects for CO_2 hydrogenation of MOFs or MOF-derived materials.

2. Confined Synthesis and Confinement Effects of MOFs as Host Materials

MOFs represent a frontier in advanced host materials for CO_2 hydrogenation due to their tunable properties including: (1) semi-rigid and highly porous structures, (2) high physical and chemical host stability, (3) strong interaction for the stable dispersion of active species, and (4) solid Lewis or Brønsted acid characteristic. These properties provide an opportunity to synthesize stable and active catalysts using MOFs as host materials in CO_2 hydrogenation. In this section, various synthetic strategies for MOF-confined molecular complexes, single atoms, NPs, or even micro-scale oxides were systematically summarized, including a one-pot synthetic approach (active sites confined in MOF cavities or channels), post-synthetic modification (active sites interacting with functional cavities or channels), and a two-step synthetic approach (active species surrounded by MOF membranes). For further details regarding the synthesis and characterization of various MOFs, the readers are referred to previous reviews and literature cited herein [62,63]. Moreover, the corresponding catalytic performance affected by confinement effects are detailed, indicating that rational designs of the structures of MOFs and active sites are essential in the valorization of CO_2.

2.1. Molecular Complex Encapsulation in MOFs

Compared with heterogeneous CO_2 hydrogenation conducted at higher temperature and pressure conditions (e.g., >200 °C and >3 MPa), homogenous molecular complexes can work at mild conditions (e.g., <150 °C) [64]. The well-defined structures of molecular complexes facilitated the interpretation of reaction mechanisms at the molecular level, which promotes the optimization of catalyst design. A remaining challenge for applying

molecular complexes is their immobilization to fabricate stable and recyclable catalysts for practical applications. The porosity and highly ordered structure of MOFs enable their potential as ideal host materials to improve the accessibility of catalytic sites, which also makes molecular complexes recyclable and productive.

The pioneering studies by Yoshio and coworkers demonstrated that homogeneous ruthenium–phosphine catalysts could selectively catalyze CO_2 hydrogenation to formic acid at low temperatures [65]. Moreover, homogeneous molecular complexes containing n-heterocyclic carbenes (NHCs) or phosphorus–nitrogen–phosphorus (PNP) pincer-type ligands could facilitate CO_2 hydrogenation due to the strong electron-donating ability, where the Ru PNP-pincer catalyst could deliver a turnover frequency (TOF) value of 1,100,000 h^{-1} at 65 °C and 4 MPa (H_2/CO_2 (v/v) = 3:1) [66–70]. However, the challenges including catalysts and products separation and recyclability hindered their industrial applications. Accordingly, the heterogenization of molecular complexes is an effective pathway, which could integrate the distinctive activity of homogeneous catalysts with the advantages of heterogeneous catalysts [71,72]. MOFs are the potential candidates to host molecular complexes. For example, Wu et al. reported various heterogeneous Ru-based molecular complexes immobilized on an azolium-based MOF via post-synthetic metalation which were examined for CO_2 hydrogenation toward formic acid, as shown in Figure 2. The examined Ru molecular complexes included $RuCl_3$, $[RuCp^*Cl_2]_2$ (Cp* = pentamethylcyclopentadienyl), and $[Ru(C_6Me_6)Cl_2]_2$ (C_6Me_6 = hexamethylbenzene); the corresponding hybrid catalysts were named Ru$_x$-NHC-MOF (x = 1, 2, 3). The surface areas and total pore volumes of the three as-prepared catalysts decreased due to the occupancy in the MOF pores (Figure 2b). The as-obtained Ru$_3$-NHC-MOF catalyst exhibited the highest activity due to the stronger electron-donating ability of the C_6Me_6 ligand in the $[Ru(C_6Me_6)Cl_2]_2$ complex. Specifically, values of the turnover number (TON) up to 3803 were obtained at 120 °C under a total pressure of 8 MPa (H_2/CO_2 (v/v) = 1) for 2 h in the presence of K_2CO_3 as the base in N, N-Dimethylformamide (DMF) solvent. The strong polarity of the DMF solvent also facilitated the insertion of CO_2 into the Ru−H bond, which is the rate-determining step (RDS) for CO_2 hydrogenation [73].
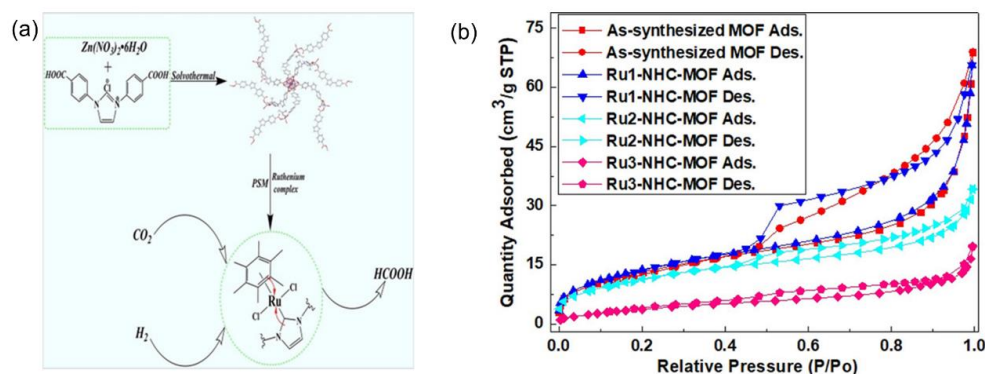

Figure 2. (**a**) Ruthenium complexes confined in an azolium-based MOF for selective CO_2 hydrogenation to formic acid. Reproduced with permission. (**b**) N_2 adsorption–desorption isotherms of as-synthesized MOF, Ru$_1$-NHC-MOF, Ru$_2$-NHC-MOF, and Ru$_3$-NHC-MOF catalysts. Reproduced with permission [73]. Copyright 2018, Wiley-VCH.

Host (MOF)-guest (molecular complexes) composites have already demonstrated their advantages in CO_2 hydrogenation. However, the successful synthesis of host–guest composites is limited, and they can only be prepared via de novo synthesis and post-synthetic modification [49,74,75], where the size of molecular complexes should be smaller than the pore of MOFs. Recently, the Tsung group developed a post-synthetic approach to synthesize host–guest composites, where guest molecular complexes were larger (e.g., 3–4 times) than the aperture size of the MOF host but could also be encapsulated into MOFs via aperture-opening events [50]. Guest molecular complexes were encapsulated

effectively due to the short-lived "open" states of the pores formed upon linker dissociation, which circumvented the disadvantages of previous strategies including tedious synthetic processes and poor encapsulation efficiency. The aperture-opening process occurred even in the robust MOF, which was significantly affected by the identity of the selected solvent, as shown in Figure 3. A Zr-based MOF consisting of a cubic framework of cationic $Zr_6O_4(OH)_4$ nodes and 1,4-benzenedicarboxylate linkers (BDC) was selected as the host material, named UiO-66. The (tBuPNP)Ru(CO)HCl (tBuPNP = 2,6-bis((di-tert-butyl-phosphino)methyl)pyridine) was successfully encapsulated into UiO-66 (named [Ru]@UiO-66) by exposing UiO-66 to methanol solvent containing (tBuPNP)Ru(CO)HCl at 55 °C for 5 days in Figure 3. [Ru]@UiO-66 exhibited a comparable TON of ca. 280,000 with that of homogeneous molecular catalysts for CO_2 hydrogenation to formic acid in DMF at 27 °C and 1.5 MPa (H_2/CO_2 (v/v) = 4:1). Interestingly, the recyclability and stability of the encapsulated composites were much better than those of homogeneous ones, where the activity of [Ru]@UiO-66 was maintained after five successive cycles. The homogeneous composite lost more than half of its original activity in the second cycle, which was likely due to the biomolecular deactivation [48].
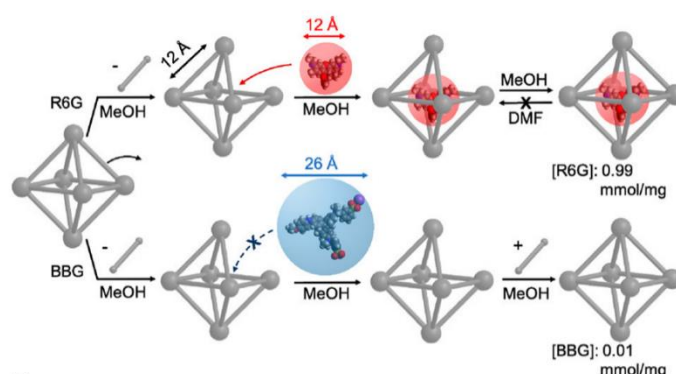

Figure 3. Encapsulation of molecular complexes (R6G or BBG) in UiO-66 in methanol and DMF at 55 °C for 5 days. Reproduced with permission [48]. Copyright 2018, American Chemical Society.

Apart from formic acid as the main product during CO_2 hydrogenation, CH_3OH also could be produced on MOF-confined molecular complexes. Inspired by biological organisms [76,77], Rayder et al. developed a multi-component catalyst system by integrating [Ru]@MOF and another Ru molecular catalyst to achieve a three-step cascade CO_2 hydrogenation toward CH_3OH. More specifically, the molecular complexes (tBuPNP)Ru(CO)-HCl (Ru-1) were firstly encapsulated within the pores of UiO-66 (named Ru-1@UiO-66) by the aperture-opening strategy, where Ru-1 served as an active site to hydrogenate CO_2 to formic acid [71], and the zirconium oxide nodes with Lewis acidity in UiO-66 served as active sites to catalyze formic acid to a formate ester [78]. Then, another homogenous Ru-based complex (tBuPNN)RuH(CO)Cl (Ru-2) was necessary to catalyze ester hydrogenation to CH_3OH, as illustrated in Figure 4a [79]. This multi-component catalyst system could deliver a TON of 4710 ± 150 in DMF in the presence of ethanol at 70 °C and 4 MPa (H_2/CO_2 (v/v) = 37:3) after 16 h. In contrast, Ru-1, UiO-66, or Ru-2 ([Ru-1, Ru-2]@UiO-66) were found to be inactive, when independently or physically mixed for CO_2 hydrogenation. More interestingly, the co-encapsulation of Ru-1 and Ru-2 in UiO-66 was also prepared successfully, which exhibited higher activity toward CH_3OH than that of mixtures of Ru-1@UiO-66 and Ru-2@UiO-66 as shown in Figure 4b. Even though some activity loss was observed over [Ru-1, Ru-2]@UiO-66, the durability was enhanced and no significant loss was found during the five successive cycles, which was likely due to the isolated sites achieved by the MOF avoiding possible bimolecular decomposition pathways [51]. In this study, UiO-66 not only served as the host material, but also provided a solid Lewis site to transform formic acid to formate ester.
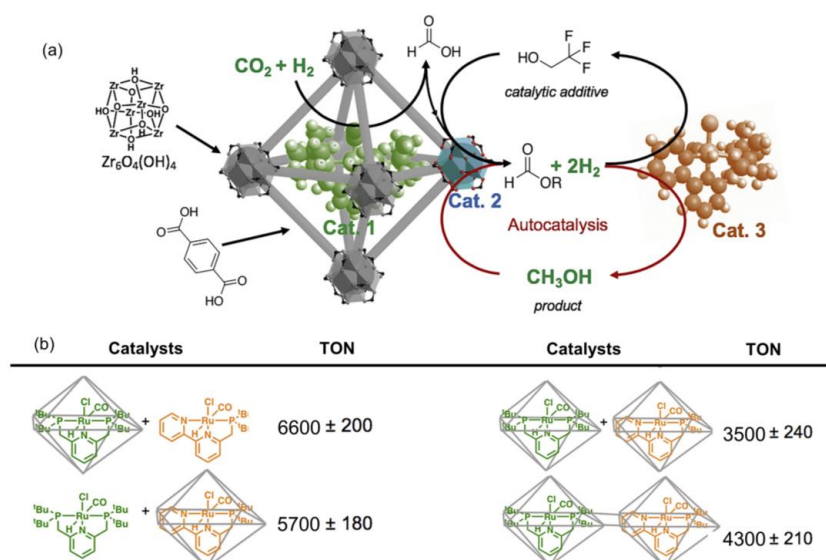
Figure 4. (**a**) The scheme of cascade hydrogenation of CO_2 to CH_3OH on MOF–molecular complex host–guest composites. (**b**) The turnover number (TON) was summarized over various kinds of hybrid composites. Reproduced with permission [51]. Copyright 2020, Elsevier Inc. 2020.

Beyond the primary coordination sphere, second-sphere interactions in host–guest multicomponent catalysts also significantly affect the catalytic activity and selectivity [80–86]. Tsung and coworkers extensively investigated the second sphere interactions in multicomponent catalyst systems by combining ligand design in the MOFs and the aperture-opening encapsulation strategy for CO_2 hydrogenation to CH_3OH [52]. The structure–activity relationships during CO_2 hydrogenation were efficiently established using various functionalized UiO-66-X hosts (X = -CH_3, -F, -Br, -NO_2, -NH_2, and -NH_3^+), as shown in Figure 5, where the UiO-66-NH_3^+ host was found to significantly increase CH_3OH activity compared with that utilized by other UiO-66-Xs as the host. Mechanistic experiments revealed that the NH_3^+ functionality could serve as Brønsted acid and facilitate the CO_2 hydrogenation to formic acid with autocatalytic features. Importantly, the synergistic effect from the host worked only when the functional group was physically close to the encapsulated molecular complexes. The combination of Ru-1@UiO-66-NH_3^+ and Ru-2@UiO-66 could achieve the highest TON of 10,900 at 70 °C and 4 MPa (H_2/CO_2 (*v*:*v*) = 37:3) in molecular sieves treated with DMF with 10^{-5} mmol 2,2,2-trifluoroethanol after 16 h [52].
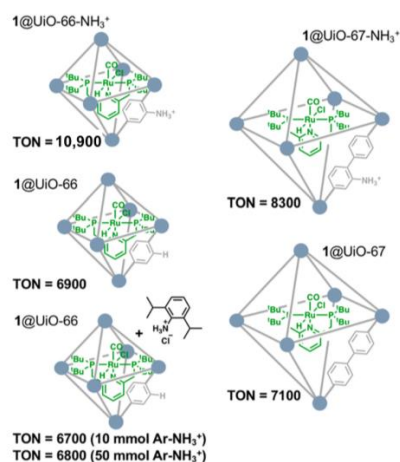

Figure 5. Effect of the pore size of the MOF cage (UiO-66 and UiO-67) and external anilinium functional groups on turnover number (TON) for CO_2 hydrogenation to CH_3OH at 70 °C and 4 MPa (H_2/CO_2 (*v*/*v*) = 37:3). Reproduced with permission [52]. Copyright 2018, American Chemical Society.

Despite the above advances, it still remains challenging to realize the precise control of the position of molecular complexes in MOFs [52,87–90]. To achieve the controllable modulation of the local environment of active sites in MOFs, organic linkers with some functional groups have been introduced to anchor the metal ions [75,91,92], mimicking ligands in organometallic complexes to stabilize homogeneous organometallic complex catalysts in a solid matrix [93]. An et al. reported a novel heterogenized molecular catalyst for CO_2 hydrogenation to formic acid via incorporating Ir^{III} ions into UiO-type MOFs using post-synthetic metalation followed by $NaBhEt_3$ treatment, where 2,2′-bipyridine-5,5′-dicarboxylate ligands (bpydc) with or without −OH substitution of the 6-position were synthesized, as shown in Figure 6a. The TON of as-obtained bpydcOH-Ir^{III}-UiO and bpydc-Ir^{III}-UiO achieved 6149 and 417 at 85 °C and 0.1 MPa (H_2/CO_2 (*v*:*v*) = 1:1) over 15 h, respectively. The isotopic effect and DFT calculations revealed that concerted proton–hydride transfer was the RDS of CO_2 hydrogenation. Then, the electron-donating groups from -OH and the pyridyl nitrogen were ascribed to facilitate the RDS [94]. Tshuma et al. presented the rational design and synthesis of novel isostructural MOFs containing catalytically active Pd(II) sites by using 2,2′-bipyridine-4,4′-dicarboxylate linkers, named (Mg(bpdc)(DMF)$_2$PdCl$_2$]n (Pd@Mg:JMS-2) and [Mn(bpdc)(DMF)$_2$PdCl$_2$]n (Pd@Mn:JMS-2)), respectively. Figure 6b shows the packing diagram and channel structure of Pd@Mg:JMS-2. For CO_2 hydrogenation to formic acid in ethanol with KOH as the base at 100 °C and 5 MPa (H_2/CO_2 (*v*:*v*) = 4:1), Pd@Mn:JMS-2 and Pd@Mg:JMS-2 gave the TOF values of 409 h^{-1} and 303 h^{-1}, respectively, which were higher than that of the homogeneous complex of 170 h^{-1} (Pd directly anchored on 2,2′-bipyridine-4,4′-dicarboxylate). The presence of open metal sites and the encapsulation effect are beneficial to concentrate the CO_2 and H_2 gases and avoid deactivation. The reaction mechanism was proposed as follows: (1) H_2 was first activated to form Pd-dihydride intermediate; (2) the Pd-hydride complex attacked CO_2 to generate the formate complex, then desorbed to regenerate the active sites [95].
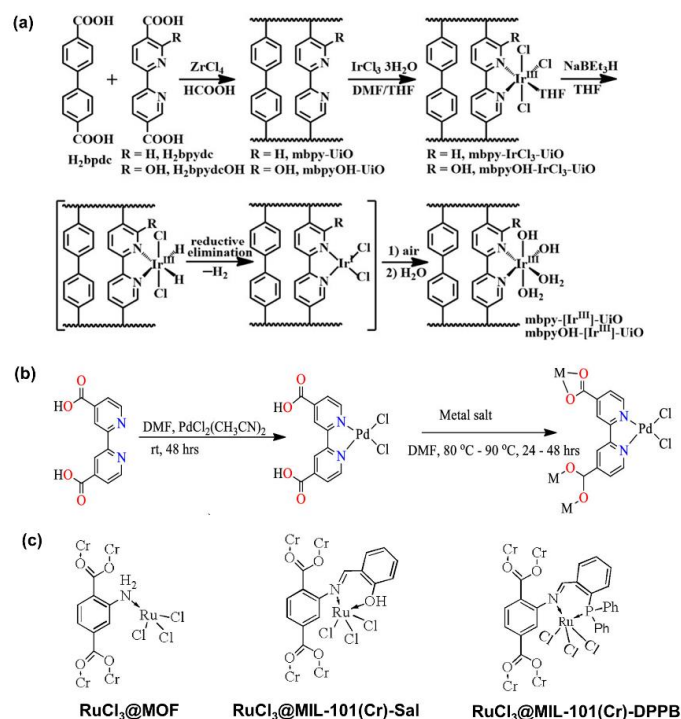

Figure 6. (**a**) The scheme of the host–guest composites (mbpyOH-[Ir^{III}]-UiO and mbpy-[Ir^{III}]-UiO) preparation. Reproduced with permission [94]. Copyright 2017, American Chemical Society. (**b**) The scheme of the host–guest composite (Pd@Mg:JMS-2). Reproduced with permission [95]. Copyright 2020, American Chemical Society. (**c**) The molecular structure of the as-prepared Ru-based catalysts. Reproduced with permission [96]. Copyright 2019, Elsevier.

It was also noticed that different linkers could significantly affect the catalytic performance during CO_2 hydrogenation. Wang et al. successfully immobilized Ru-based molecular complexes into terminal amino functionalized MIL-101(Cr)-NH_2 by post-synthetic modification, where salicylaldehyde (Sal) and 2-diphenylphosphinobenzaldehyde (DPPBde) were utilized as bridging linkers between MOF and Ru (III) ions. The structure of active sites is shown in Figure 6c, where $RuCl_3$ coordinated with the amino group in the MIL-101 (Cr)-NH_2 ($RuCl_3$@MOF), the N atom of carbon–nitrogen double bonds and the O atom of Sal ($RuCl_3$@MIL-101(Cr)-Sal), and the N atom of carbon–nitrogen double bonds and the P atom from linker DPPBde ($RuCl_3$@MIL-101(Cr)-DPPB), respectively. Among them, $RuCl_3$@MIL-101(Cr)-DPPB delivered the highest TON of 242 under 120 °C and 6 MPa (H_2/CO_2 (*v:v*) = 4:1) with triethylamine (Et_3N) as the base in ethanol during CO_2 hydrogenation toward formic acid. Mechanistic insights suggested that the stronger electron-donating ability of P sites in DPPBde promoted the RDS, namely, the insertion of CO_2 into Ru-H [96]. Similarly, ZIF-8 was also utilized as the host, and 3-methyl-1,2,4-triazole with uncoordinated N sites was introduced to anchor Ru by post-synthetic modification, which was examined for CO_2 hydrogenation to formic acid. The donated electron to Ru from uncoordinated N sites in linkers decreased the activation energy of CO_2 activation, as revealed by experiments and theoretical calculations [97].

Overall, the host–guest composites not only maintain the distinctive activity in low-temperature CO_2 hydrogenation and increase the stability and recyclability of molecular complexes but also provide a platform to further enhance their activity and/or selectivity via engineering the primary coordination sphere and second sphere interactions. The one-pot synthesis is relatively simple to encapsulate molecular complexes into an MOF cage or channel, but it is limited by the size of the MOF channel and remains challenging to tune the encapsulation location and uniformity. It is worth noting that guest molecule leaching always hinders this kind of catalyst in large-scale applications. The post-synthetic modification via the aperture-opening strategy could break the limitation of the MOF channel and guest molecule leaching, but the underlying mechanism remains elusive, impeding the rational design. Moreover, these strategies are applicable only after sophisticated synthetic techniques to construct the desired structure, which would limit large-scale applications. Thus, the development of novel and efficient strategies to prepare MOF-based host–guest composites is highly desired.

2.2. Active NPs Confined into MOFs' Cavities or Channels

Nanometals or oxides have been demonstrated to be effective catalysts for CO_2 hydrogenation [3,98,99]. Nanoscale effects have been well examined in the rational design of high-performance catalysts due to their specific structural and electronic effects (e.g., facet, coordination, or unsaturated sites) [58,100,101]. High surface-area supports (e.g., zeolite, carbon, oxide, and MOF) are needed to stabilize active sites due to their thermodynamic instability at the nano-/atomic scale, especially at high temperature and pressure conditions in the presence of H_2O. Among them, the active sites confined in MOFs provide more opportunities, resulting from their chemically tunable pore surfaces [102], framework flexibility [103], and various modification strategies (e.g., post-synthetic modification and exchangeable ligands) [104,105]. Apart from active NPs directly confined in MOFs, the functionalization of linkers with catalytically active species [93,106] and utilization of the modified MOF nodes as the active sites [107] were also designed. The functionalized linkers with different chemical groups could also enhance reactant adsorption [108,109], promoting CO_2 hydrogenation. In this section, the strategies for MOFs confined in NPs catalysts will be reviewed and the confinement effects will be presented, including size effects, encapsulation effects, and synergistic effects, to provide deeper insights into the advantages and features of confined catalysis.

2.2.1. Atomically Active Sites Confined in MOFs

The electronic and geometric structures of supported NPs can result in dramatic changes in catalytic performance [110–114]. Atomically active sites have been well studied for hydrogenation reactions due to their unique electronic and geometric structures, 100% atom utilization, and unique reaction micro-environments [115–118]. Recent theoretical and experimental studies have found that atomically active sites exhibit better catalytic activity or selectivity than their nanometer-sized counterparts [118–120]. Moreover, the rapid development of related synthetic strategies, characterizations, and theoretical interpretation of atomically active sites provide an ideal platform to understand the structure–performance relationship and reaction mechanisms.

A unique example is that a well-defined MOF containing functionalized linkers with catalytically active species was utilized as a model material to interpret the reaction mechanism during CO_2 hydrogenation to examine the structural requirements for CH_3OH production on $ZrZnO_x$. The well-defined Zn^{2+}–O–Zr^{4+} sites were constructed by post-synthetic treatment of $Zr_6(\mu_3\text{-O})_4(\mu_3\text{-OH})_4$ nodes of MOF-808 with $ZnEt_2$ and then followed by a mild thermal treatment to remove capping formats on Zr SBUs. The as-prepared composites delivered a high CH_3OH yield of 5.72 $mmol_{CH3OH}$ g_{Zn}^{-1} h^{-1}, >99% CH_3OH selectivity, and excellent stability (e.g., >100 h) in CO_2 hydrogenation at 250 °C. A synergistic effect between open Zr^{4+} sites and Zn^{2+} centers was proven to be indispensable to the generation of CH_3OH. Mechanistic investigations disclosed that (1) Zn^{2+} was responsible for H_2 activation by TPD of H_2 and H/D exchange tests; (2) CO_2 was adsorbed and activated on open Zr^{4+} sites in the nearby Zr^{4+}–O–Zn^{2+} interface, as shown in Figure 7. In situ DRIFT and DFT calculations further showed that the activated CO_2 reacted with the heterolytic splitting H^- to form *HCOO intermediate on Zn^{2+} sites, followed by hydrogenation to dioxomethylene (*H_2COO), formaldehyde (*H_2CO), methoxy (*H_3CO), and finally methanol [121]. These findings demonstrated that Zn was active for H_2 activation; meanwhile, both Zn and Zr participated in CO_2 activation, in agreement with previous studies [10,31,122]. Moreover, this study revealed the precise chemical structures of Zn and Zr in their active forms during CO_2 hydrogenation.
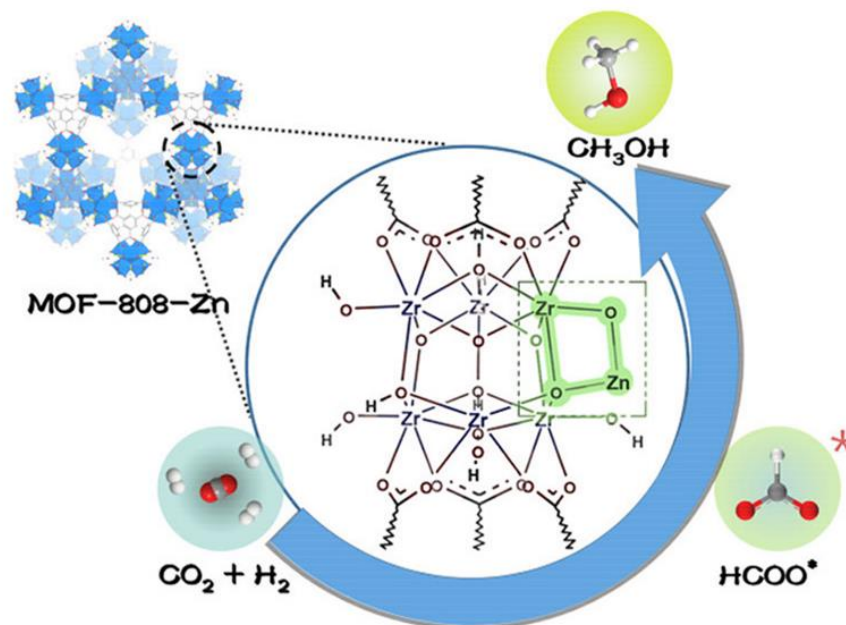

Figure 7. The scheme of neighboring Zn–Zr sites in a metal–organic framework for CO_2 hydrogenation and HCOO is the important intermediate. Reproduced with permission [121]. Copyright 2021, American Chemical Society.

Multifunctional sites in MOFs were also facilitated, enabling cascade CO_2 hydrogenation to multi-carbon products (e.g., C_2H_5OH and C_2H_4). An et al. designed well-defined Cu active sites on deprotonated $[Zr_{12}O_8(\mu_3\text{-}O)_8(\mu_2\text{-}O)_6(\text{carboxylate})_{18}]_{14}^-$ SBUs in the Zr_{12}-MOF for selective CO_2 hydrogenation to ethanol [123]. Regarding the synthesis, Zr_{12}-SBUs with an average thickness of 50 nm were prepared and the SBUs were deprotonated by $LiCH_2SiMe_3$, followed by metalation with $[Cu^I(CH_3CN)_4](BF_4)$, which was confirmed by infrared (IR) spectrum. Two types of Cu species were formed: 1) four-coordinated tetrahedral Cu^I centers($[(\mu_4\text{-}O^-)(\mu_2OCO\ \text{carboxylate})_2\ Cu^I(THF)]$) (site 1, 3) and $[(\mu_4\text{-}O-Li^+)(\mu_3\text{-}O-)(\mu_4\text{-}O-)Cu^I(THF)]$ (site 2), as shown in Figure 8. Moreover, different alkali cations were also introduced into the MOF structure to modify the local environment of Cu, which was confirmed by XAS analysis. Among them, the Cs^+-modified MOF catalyst achieved a TON of 4080 and >99% selectivity of ethanol in supercritical CO_2 (30 MPa CO_2 /5 MPa H_2) at 85 °C. In contrast, the randomly supporting active Cu sites on ZrO_2 preferred CH_3OH formation under identical reaction conditions, as the aggregation occurred. The experimental results and DFT calculations disclosed that the H_2 was activated on $(Cu^I)_2$ sites by a bimetallic oxidative addition process to form $(Cu^{2+}\text{–}H^-)_2$ and then reacted with CO_2 to produce methanol and *CHO species, where electron-rich Cu^I induced by the effective electron-donating effect of Cs could facilitate these steps. The C–C bond was formed to get the CH_3CHO intermediate via the nucleophilic attack on methanol by the CHO intermediate on bimetallic Cu sites; ethanol was formed by further hydrogenation. Additionally, alkali metals could stabilize *CHO intermediate to direct the C_2H_5OH formation. Overall, the synergistic effect between the cooperative nature of the bimetallic Cu^I_2 centers and the electron-rich environment for the Cu center was interpreted to contribute to the higher activity for C_2H_5OH formation.
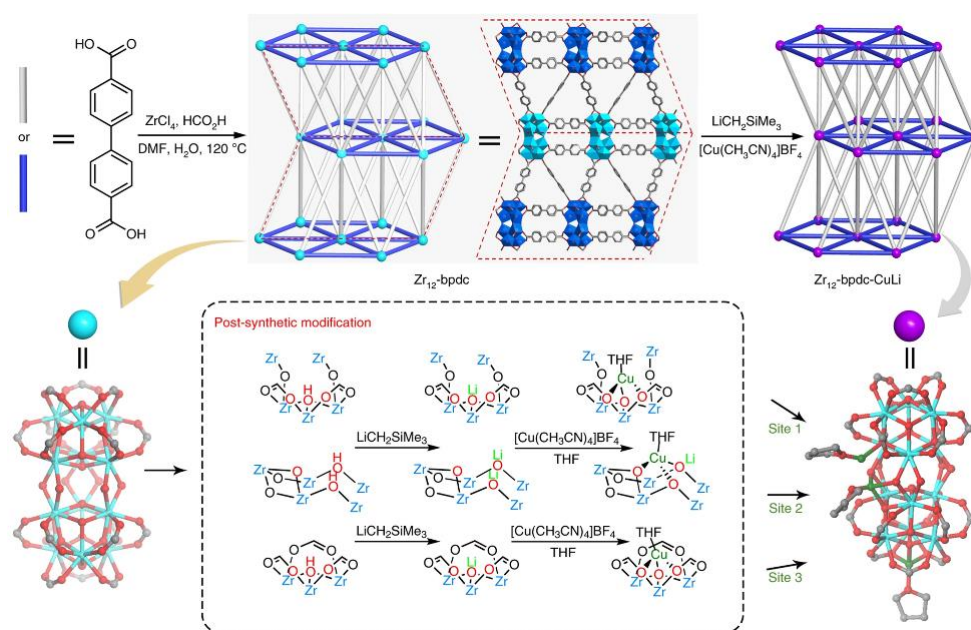

Figure 8. Synthesis and structures of Zr_{12}-bpdc and Zr_{12}-bpdc-CuLi catalysts. Reproduced with permission [123]. Copyright 2019, Nature publishing group.

To better understand the multi-functionality of MOFs, MOFs involved in catalytic cycles were also investigated. For example, Zeng et al. developed a cascade catalyst, Cu^I centers supported on MIL-125 ($[Ti_8(\mu_2\text{-}O)_8(\mu_2\text{-}OH)_4(BDC)_6]$), where the Cu^I catalyzed CO_2 hydrogenation to C_2H_5OH, but C_2H_5OH dehydration on $Ti_2\text{-}\mu_2\text{-}O–M^+$ ($M^+ = H^+$, Li^+) sites occurred. The post-synthetic metalation of SBUs was utilized for catalyst preparation and MIL-125-NH_2-Cu^I-4 was obtained, as shown in Figure 9a [124,125]. The as-obtained composites exhibited >90% selectivity toward C_2H_4 during CO_2 hydrogenation with a reaction

rate of up to 514 μmol g_{cat}^{-1} h^{-1} at 100 °C and 5 MPa (H_2/CO_2 = 3:1) in THF. The choice of MIL-125 as the support was critical to the tandem CO_2-to-C_2H_4 transformation: (1) the $Ti_8(\mu_2$-$O)_8(\mu_2$-$OH)_4$ SBU rather than other SBUs stabilized Cu^I to avoid Cu^0 formation; (2) the short Cu^I–Cu^I distance in $Ti_8(\mu_2$-$O)_8(\mu_2$-O-$CuI)_4$ enhanced the synergistic effect on C_2 formation; (3) the strong Lewis acid Ti^{IV} catalyzed C_2H_5OH dehydration at low temperatures (∼100 °C); and (4) C_2H_5OH was easily adsorbed on the $Ti_2(\mu_2$-O-$M^+)$ site in $Ti_8(\mu_2$-$O)_8(\mu_2$-O-$CuI)_4$, which further induced β-elimination to produce C_2H_4 (Figure 9b,c). This work highlighted new opportunities in using MOFs as novel supports for CO_2 hydrogenation to C_2H_4 [126]. Moreover, this study indicated the pore-dependent activity and selectivity during CO_2 hydrogenation in tunable and ordered structure MOFs.
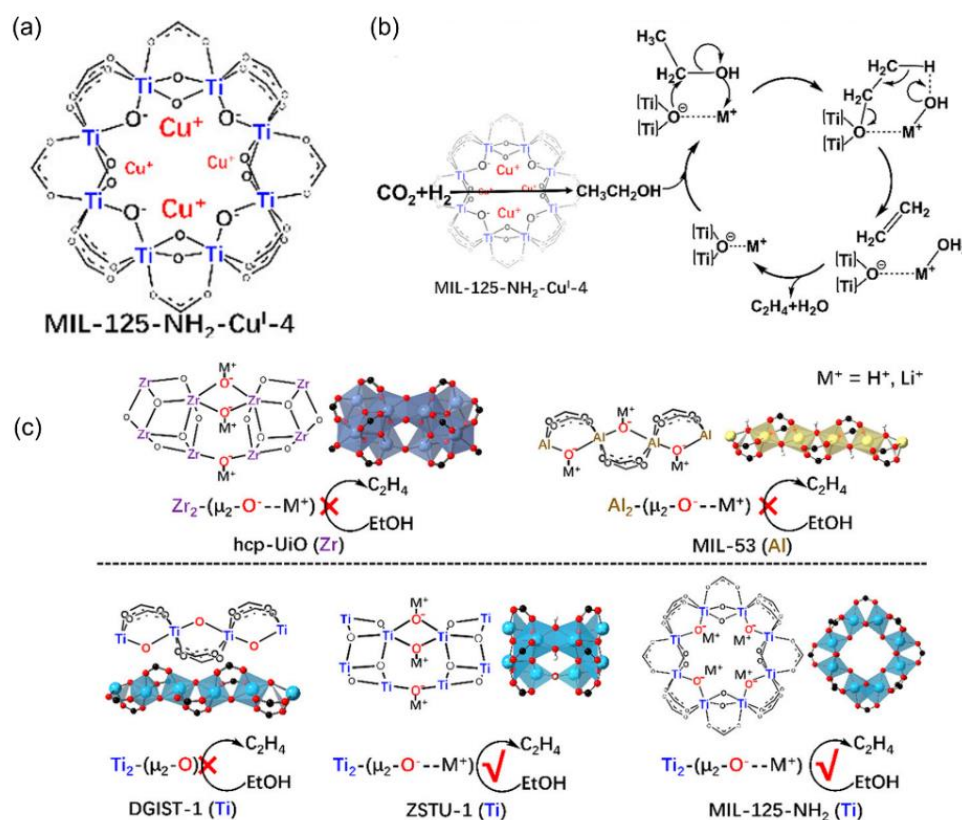

Figure 9. Multiple Cu^+ supported on a MIL-125 catalyze CO_2 hydrogenation to C_2H_4. (**a**) The local structure of catalyst. (**b**) The scheme of the tandem reaction and the ethanol dehydration mechanism. (**c**) Scheme of the C_2H_5OH conversion capability of different MOFs and their derivatives. Reproduced with permission [126]. Copyright2021, American Chemical Society.

Apart from the transition metals (Zn or Cu), noble metals (e.g., Pt) are also able to encapsulate into MOFs, where the atomically dispersed Pt_1 atom was coordinated by four O atoms in MIL-101, as shown in Figure 10a. The active sites created by metal–ligand cooperativity led to the dissociation of H_2 to form hydroxyl groups, attacking CO_2 to produce the key intermediates of HCOO*, evidenced by DFT calculations and operando spectroscopies (Figure 10b). In contrast, the Pt cluster (Pt_n) encapsulated in MIL-101 preferred hydride formation and then hydrogenated CO_2 into COOH* as key intermediates. The divergence in reaction paths resulted in different catalytic selectivity between Pt_1@MIL-101(90%) and Pt_n@MIL-101 (58%), where the *HCOO intermediates went through stepwise hydrogenation to produce CH_3OH, while *COOH was hydrogenated into various products including HCOOH, CH_3OH, CO, and CH_4 (Figure 10c,d) [127].
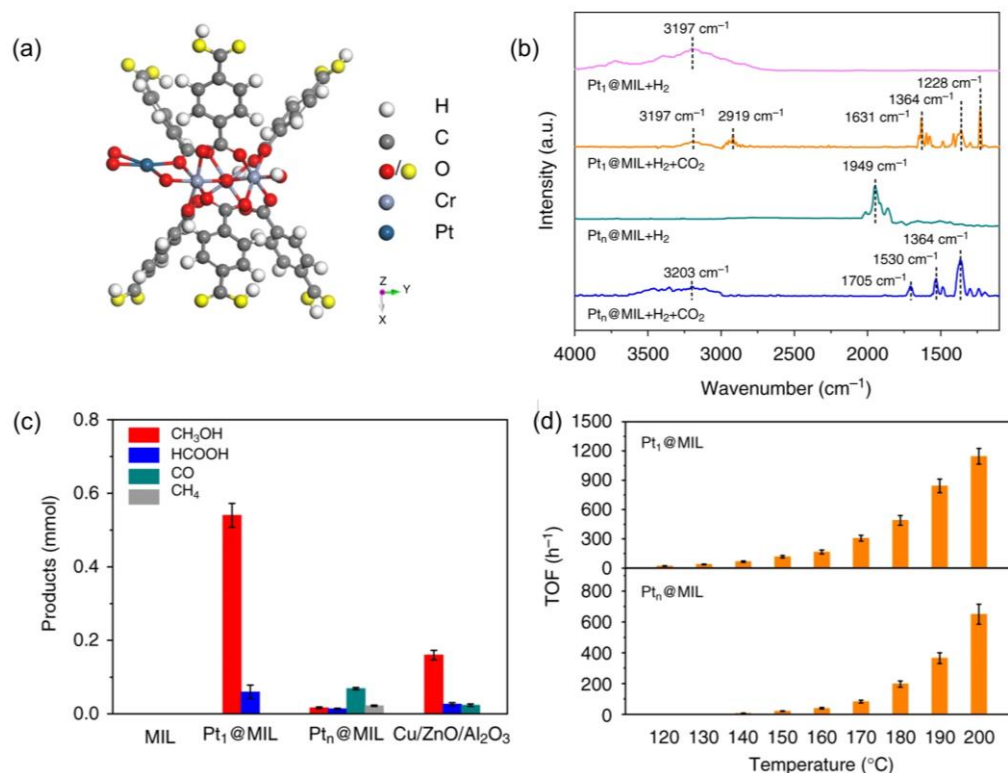
Figure 10. (**a**) Structural model of Pt_1@MIL. (**b**) The in situ DRIFT of CO_2 hydrogenation over Pt_1@MIL. (**c,d**) The comparison of catalytic performance over various catalysts during CO_2 hydrogenation. Reproduced with permission [127]. Copyright 2019, Nature publishing group.

Accordingly, atomically dispersed active sites in MOFs are an ideal target in catalyst design, especially for noble metals, which not only increase the exposed active sites per molar amount of metals but also create new prospects for the controllable surface free energy of the metal atoms. The synergistic effect in MOFs is of great importance for the rational design of catalysts to achieve excellent performance for desired products. The design of atomically distributed active metals in MOFs with reasonable catalytic performance has been demonstrated in the lab; however, no related application was found on a large scale, hence, more efforts should be directed to developing more efficient strategies for confined catalysts using MOFs as hosts.

2.2.2. Active NPs Confined in Monocrystal MOF

Heterogeneous catalysts are usually prepared by loading active metal sites onto a support, where both the structure of active metal sites (e.g., facet, morphology, and electronic state) and properties of supports (physical properties and chemical properties) will affect the catalytic performance [116,128–133]. For example, the different facets of active NPs result in different unsaturated metal surface atoms, which can change the catalytic processes; the supports not only affect the dispersion of active NPs but also tune the electronic and/or geometrical structure of active NPs via SMSI [132,134–136]. Actually, the sintering under harsh reaction conditions due to Ostwald ripening or particle migration and coalescence makes it challenging for industrial application [137,138]. An efficient and sustainable strategy, encapsulation has been well investigated to increase their long-term stability [139].

Rungtaweevoranit et al. successfully synthesized single nanocrystalline UiO-66 encapsulated 18 nm Cu via the bottom-up method using $Zr(OPr^n)_4$ as a precursor (Figure 11a,b). The as-prepared Cu@UiO-66 was demonstrated to be active and selective for CO_2 hydrogenation toward CH_3OH, and the TOF was 3.7×10^{-3} s^{-1} at 175 °C and 1 MPa ($H_2/CO_2 = 3/1$). The formation rate of CH_3OH on Cu@UiO-66 was almost two and nine times higher than

those of Cu supported on UiO-66 and commercial Cu/Zn/Al$_2$O$_3$, respectively. Moreover, 100% selectivity was observed on Cu@UiO-66. The strong interaction between Cu NPs and Zr oxide SBUs of the MOF was interpreted as leading to the higher catalytic performance [140]. Kobayashi et al. investigated the coated effects of MOFs including ZIF-8, MIL-100, and functionalized UiO-66 on CO$_2$ hydrogenation for CH$_3$OH formation, as shown in Figure 11c. The charge transfer was observed between Cu and MOF substrates, and UiO-66 was found to be the most active support. Interestingly, the replacement of Zr^{4+} with Hf^{4+} or functional groups (e.g., from -NH$_2$ to -COOH) in UiO-66 enhanced the rate of CH$_3$OH production [141]. Truhlar and coworkers provided deeper insight into the molecular interactions between Cu and Zr in UiO-66. The experimental and theoretical results disclosed that the direct interaction between Cu NPs and ZrO$_2$ nodes was essential for CO$_2$ hydrogenation to CH$_3$OH (Figure 11d) [142]. The quantitative effects of the missing-linker defects on H$_2$ and CO$_2$ activation were carried out using a detailed quantum mechanical study. It was found that the optimum number of missing linkers (ca. 5–7 per unit cell) balanced the steric effects and the strong CO$_2$ binding on the ZrO$_2$ node delivered a maximum TOF of CH$_3$OH formation [143].
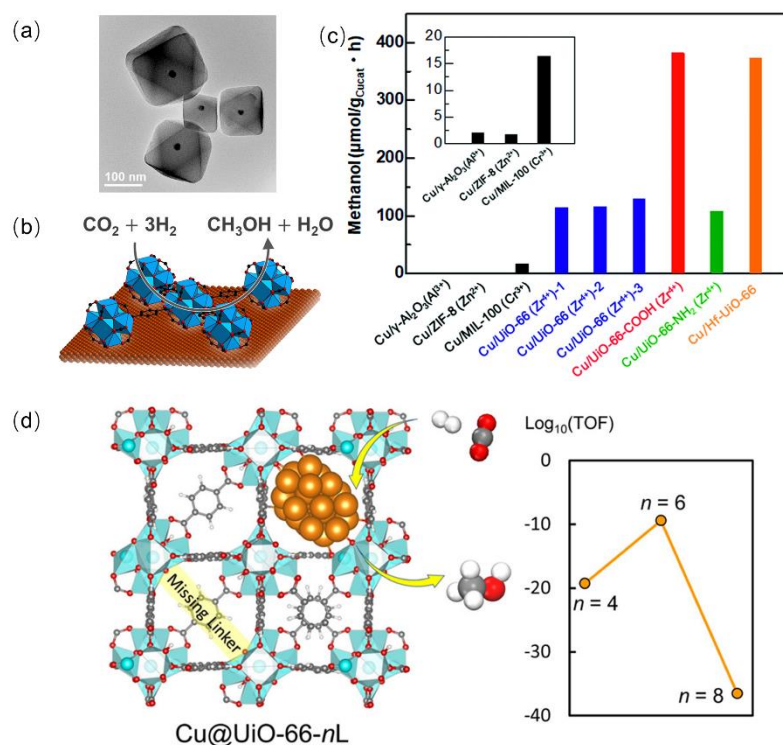

Figure 11. (**a**) TEM image of Cu@UiO-66. (**b**) The scheme of CO$_2$ hydrogenation over Cu@UiO-66. Reproduced with permission [140]. Copyright 2016, American Chemical Society. (**c**) The amount of CH$_3$OH synthesized from CO$_2$ and H$_2$ using Cu/γ-Al$_2$O$_3$ and various Cu/MOF composite catalysts. Reproduced with permission [141]. Copyright 2019, Royal Society Chemistry. (**d**) The structure–performance relationship of Cu@UiO-66 during CO$_2$ hydrogenation. Reproduced with permission [143]. Copyright 2022, American Chemical Society.

MOFs further provide a specific platform for NPs including protective microenvironments and functional sites. Zheng et al. reported that the core–shell monodispersed nanosphere Au@Pd could be encapsulated by the UiO-66 membrane to protect its morphology and then the microporous characteristic of UiO-66 preferred the adsorption of Pt NPs on its surface to impart its functionality. This kind of assembly enhanced the interaction between NPs and UiO-66, allowing for the spatial distribution of NPs in MOFs. Furthermore, the catalysts for the RWGS in a fixed-bed flow reactor exhibited high catalytic activity and CO selectivity [144].

MOFs can also serve as novel supports for mixed oxide catalysts via taking advantage of tunable and specific strong metal–support interactions. Lin and coworkers demonstrated a strategy to utilize the UiO-bpy MOF constructed by bpy and $Zr_6(\mu_3-O)_4(\mu_3-OH)_4$ to encapsulate ultrasmall Cu/ZnO_x nanoparticles, which selectively catalyzed high-rate CO_2 hydrogenation to CH_3OH with the yield up to 2.59 g_{CH_3OH} kg_{Cu}^{-1} h^{-1}, 100% CH_3OH selectivity, and high stability over 100 h (Figure 12a). The UiO-bpy MOF was chosen because of its exceptional hydrothermal stability. Post-synthetic metalation was developed to introduce Cu^{2+} and Zn^{2+} ions sequentially, which were coordinated to the bpy and μ_3-OH sites in the MOF, respectively. Finally, ultra-small Cu/ZnO_x NPs generated under reaction conditions were encapsulated in the tetrahedral and octahedral cages confined by the ligands as the active sites. The as-prepared composite exhibited much better CH_3OH selectivity and stability than those of commercial $Cu/ZnO/Al_2O_3$ (Figure 12b), likely resulting from the suppression of Cu NPs' agglomeration and phase separation between Cu and ZnO_x. Regarding mechanistic understanding, the authors proposed that CO_2 was adsorbed on unsaturated ZrO_x and ZnO_x sites to form carbonates and bicarbonates; the homolytic dissociation of H on Cu spill over to the Zr sites on the SBUs and defect sites of ZnO_x (Figure 12c). Overall, the synergistic combination of hydrogen activation sites on Cu and CO_2 activation on ZnO_x and Zr SBUs contributes to superior performance of the CuZn@UiO-bpy catalyst [145]. Similarly, Yu et al. also reported that ultra-small bimetallic Cu/ZnO_x NPs was encapsulated in UiO-66 by the deposition–precipitation method; both metal loading and the Cu/Zn mole ratio could regulate the Cu-Zn interaction. The highest CH_3OH yield of 9.1% was obtained over the Cu-Zn@UiO-66 catalyst (Cu-Zn loading: 35 wt.% and Cu/Zn mole ratio: 2.5) [146].
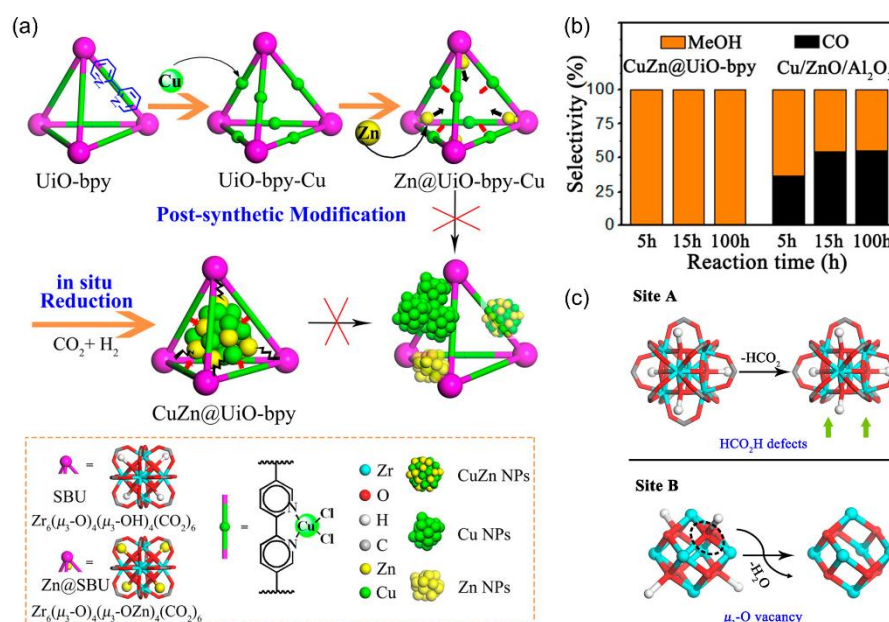

Figure 12. (**a**) The scheme of preparing CuZn@UiO-bpy via in situ reduction of post-synthetically met-alated UiO-bpy. (**b**) Selectivity of CH_3OH vs reaction time over CuZn@UiO-bpy and $Cu/ZnO/Al_2O_3$. (**c**) Formation of unsaturated Zr sites that can accept CO_2 and hydrogen spillover from Cu surfaces. Reproduced with permission [145]. Copyright 2017, American Chemical Society.

2.2.3. Active Species Confined in MOF Membrane

The active species of CO_2 hydrogenation are not only encapsulated in monocrystal MOFs, but also confined by the MOF membrane. The combination of guest species and different types of MOF active sites (e.g., metal nodes, functional organic linkers) makes MOFs promising multifunctional materials for synergistic catalysis [47]. For example, the $ZnZrO_x$/SAPO-34 composite was able to selectively catalyze CO_2 hydrogenation to paraffin. Jiang et al. shifted the product distributions from paraffins to olefins via the

introduction of the UiO-66 membrane as a coating layer on the SAPO-34 surface. It was demonstrated that the stable UiO-n membrane passivated the excessive Brønsted acid sites of SAPO-34, suppressing the hydrogenation of olefins to paraffins. Meanwhile, the uniform UiO-66 membrane had no effect on the diffusion step during CO_2 hydrogenation, where the selectivity of the C_2-C_4 olefins was increased from 57% on $ZnZrO_x$/SAPO-34 to 80% on that with a UiO-66 membrane under 380 °C, 3 MPa, and GHSV of 6000 h^{-1} (CO_2/H_2/Ar = 24:72:4), as shown in Figure 13a [147]. Compared with the existing strategies of adjusting the acidity of zeolites by changing the structure of the zeolite framework (e.g., alkali treatment or increasing calcination temperature), the method of membranization by coating a layer of a functional MOF membrane on the zeolite surface did not affect the framework structure. Moreover, a UiO-66 membrane was epitaxially grown on the surface of nano-SAPO-34 clusters as a support for dispersed Pt for CO_2 hydrogenation. The MOF membrane not only overcomes the noble metal agglomeration and enhances the molecular sieve synergistic catalysis, but also provides sites for CO_2 adsorption, significantly enhancing the selectivity and yield [148]. Similarly, Pan et al. developed a strategy for the epitaxial growth of the UiO-66-NH_2 shell to obtain an MOF-membranized bicomponent core−shell catalyst, HZSM-5@UiO-66-NH_2/Pd. By coating UiO-66-NH_2 on the surface of HZSM-5, the highly dispersed and small Pd NPs can be anchored on the HZSM-5@UiO-66-NH_2 supports owing to the affinity between UiO-66-NH_2 and Pd NPs. The as-prepared HZSM-5@UiO-66-NH_2/Pd exhibited high CO selectivity (92.2%) with 17.1% CO_2 conversion in CO_2 hydrogenation toward CO at 320 °C [149].
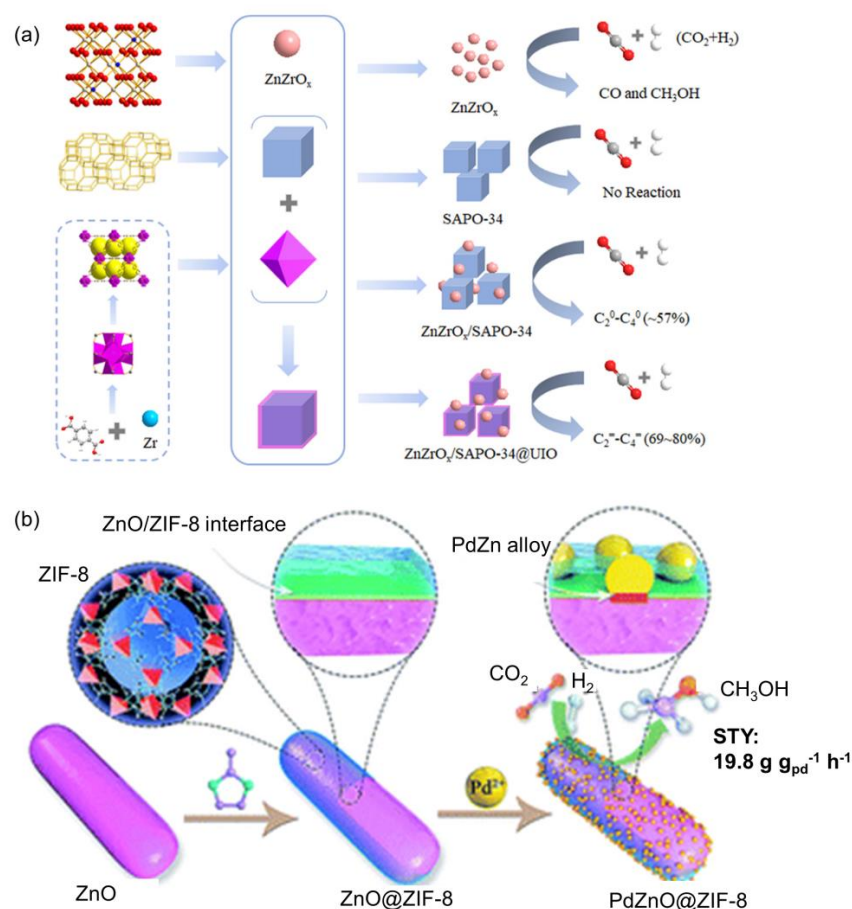

Figure 13. (**a**) The scheme of the $ZnZrO_x$/SAPO-34@MOF catalyst assembly for CO_2 hydrogenation. Reproduced with permission [147]. Copyright 2022, American Chemical Society. (**b**) Confinement of PdZn alloy in a defect-enriched ZnO/ZIF-8 interface for efficient and selective CO_2 hydrogenation to CH_3OH. Reproduced with permission [1]. Copyright 2019, Royal Society of Chemistry.

Apart from Cu/ZnO catalysts, Pd/ZnO catalysts are also active for CH_3OH production in CO_2 hydrogenation [150,151]. Li et al. designed core–shell ZnO@ZIF-8 nanorods with an ultrathin ZIF-8 membrane overcoating to confine Pd NPs at the ZnO/ZIF-8 interface for CO_2 hydrogenation, as shown in Figure 13b. Surface oxygen defects of ZnO were generated during the formation of ZIF-8 shells, which facilitated the chemisorption of CO_2 by promoting electron transfer to CO_2. Sub-nano PdZn alloy was confined at the ZnO/ZIF-8 interface after H_2 reduction, giving a high CH_3OH selectivity and long-term stability. The thickness of ZIF-8 significantly dominated the activity of CH_3OH formation, which was related to the number of PdZn alloy sites at the interface with O-defective ZnO. The optimized catalyst achieved 66–78% of CH_3OH selectivity and 12.1–19.8 g g_{Pd}^{-1} h^{-1} of methanol yield at 250–290 °C and 4.5 MPa, showing much higher values than those of reported Pd-based catalysts under comparable conditions [1].

With the rapid development of synthetic chemistry, various MOF-confined catalysts with different structures and interfaces were successfully constructed via one-pot synthesis and post-synthetic modification, which impressively exhibited unique properties over traditionally supported catalysts. The catalytic performance of various catalysts in CO_2 hydrogenation is summarized in Table 1. However, they still suffered from big challenges, especially MOF stability in fixed-bed type reactors. Most MOFs were easily decomposed in high-polar solvents or at temperatures higher than 300 °C, especially in the presence of water [152–154].

Table 1. Summary of CO_2 hydrogenation over various catalysts.

Catalysts	Reaction Conditions			Performance		Ref.
	P (MPa)	T (°C)	CO_2/H_2	TON	Product	
Ru_3-NHC-MOF	8	120	1	3803	HCOOH	[65]
[Ru]@UiO-66[1]	1.5	27	4	280,000	HCOOH	[48]
Ru-1@UiO-66+Ru-2	4	70	12	6600	CH_3OH	[79]
Ru-2@UiO-66+Ru-1				5700		
Ru-1@UiO-66+Ru-2@UiO-66				3500		
[Ru-1, Ru-2]@UiO-66				4300		
Ru-1@UiO-66-NH_3^+	4	70	12	10,900	CH_3OH	[52]
Ru-1@UiO-66				6900		
Ru-1@UiO-67				7100		
Ru-1@UiO-66-NH_3^+				8300		
bpydcOH-Ir^{III}-UiO	0.1	85	1	6149	CH_3OH	[87]
bpydc-Ir^{III}-UiO				417		
Pd@Mn:JMS-2	5	100	4	409	C_2H_5OH	[88]
$RuCl_3$@MIL-101(Cr)-DPPB	6	120	4	242	HCOOH	[89]
Zn-MOF-88	4	250	3	5.9 [a]	CH_3OH	[121]
[Cu^I]	35	85	0.2	4080	C_2H_5OH	[123]
Cu/MIL-125	5	100	3	514 [a]	C_2H_4	[126]
Pt_1@MIL-101	3.2	150	3	0.6 [a]	CH_3OH (90%)	[127]
CuNP@UiO-66	1	175	3	0.004 [b]	CH_3OH	[140]
CuZn@UiO-bpy	4	250	3	2.6 [c]	CH_3OH	[145]

Note: [Ru]: (tBuPNP)Ru(CO)HCl; Ru-1: (tBuPNP)Ru(CO)-HCl; Ru-2: (tBuPNN)RuH(CO)Cl; bpydcOH: 2,2′-bipyridine-5,5′-dicarboxylate ligands (bpydc) with −OH substitution on the 6-position; Pd@Mn:JMS-2: [Mn(bpdc)(DMF)2PdCl2]n and 2,2′-bipyridine-4,4′-dicarboxylate (bpdc); DPPB: 2-diphenylphosphinobenzaldehyde (DPPBde); a: mgCH3OH gZn^{-1} h^{-1}; [Cu^I]: [(μ_4-O−Li$^+$)(μ_3-O−)(μ_4-O−)Cu^I(THF)]; b: s^{-1}; c: g$_{MeOH}$ kgCu^{-1} h^{-1}.

3. Confined Synthesis and Confinement Effects for MOF-Derived Materials

MOFs have been explored as potential templates or precursors to prepare highly dispersed NPs via thermal decomposition due to their unique structure and textural prop-

erties [57,155–157]. Carbon-encapsulated NPs derived from MOFs as emerging catalysts received tremendous research efforts [158–160]. The framework of MOFs could protect the active site aggregation to generate highly dispersed NPs during high-temperature pyrolysis. Moreover, the confinement effects induced by the encapsulation carbon layer provide robust microenvironments for CO_2 hydrogenation, which could tune the binding energy of key intermediates and affect the adsorption of CO_2 and transportation of products. In this section, we will simply highlight some important merits of the encapsulated metal nanoparticles for CO_2 hydrogenation, including modification of local reaction environment, electronic transfer, and interfacial catalysis to enhance catalytic performance.

Carbon-encapsulated highly dispersed NPs derived from MOFs were widely investigated for selective CO_2 hydrogenation. Lu et al. reported a one-step pyrolysis of MOFs containing both an N-free and an N-containing linker to obtain highly dispersed cobalt NPs embedded in a carbon matrix for selective CO_2 hydrogenation to CO (Figure 14a,b) [161]. The presence of N in the MOF precursor could not only decrease the size of generated Co [162,163], but also modulate local reaction conditions because of the formation of a Mott–Schottky interface, which lowered the energy barrier for the formation of formate intermediates [164–166]. Similar enhancement was also observed in Fischer–Tropsch synthesis [167]. Moreover, Ni-based MOFs could generate hierarchical Ni@C hollow spheres composed of highly dispersed Ni NPs confined in carbon shells, which was active and selective for CO_2 hydrogenation to CH_4 (Figure 14c,d). The high surface area and highly dispersed active sites were ascribed to promote CO_2 adsorption and redox catalysis [168]. Apart from C_1 products, highly dispersed Fe-based catalysts derived from Fe-MIL-88B could catalyze CO_2 actively and selectively to valuable hydrocarbons (C_{2+}) [169–174]. Ramirez et al. examined the promotion effects of various elements (Cu, Mo, Li, Na, K, Mg, Ca, Zn, Ni, Co, Mn, Fe, Pt, and Rh) for the resulting Fe@C-based composites during CO_2 hydrogenation, where the Basolite F300(Fe) was used as a template and incipient wetness impregnation was utilized to add the various promotors (Figure 14e) [56]. Among them, only K could increase the activity and enhance C_2–C_6 olefin selectivity from 0.7% to 36%.

Another property of the confinement effects is the strong interaction between the metal NPs and the encapsulating materials, which facilitates the electron transfer under some conditions and maximizes the interfacial area due to their close contact [175–190] Pustovarenko et al. demonstrated the MOF-mediated route for the preparation of highly efficient Co_3O_4-supported In_2O_3 catalyst via stepwise pyrolytic–oxidative decomposition, as shown in Figure 15a, which selectively catalyzed selective CO_2 hydrogenation to CH_3OH [191]. The stable Cu-ZnO interfacial sites were also constructed using a novel bimetallic CuZn-BTC MOF for CO_2 hydrogenation to CH_3OH [192]. Additionally, Cu-based catalysts were revealed to be structure sensitive, including facet, defect, particle size, and interface [22,193–196]. Han et al. prepared hollow Cu@ZrO_2 catalysts through pyrolysis of Cu-loaded Zr-MOF, where low-temperature pyrolysis (e.g., 300 °C) produced highly dispersed Cu nanoparticles with balanced Cu^0/Cu^+ sites, larger amounts of surface basic sites, and an abundant Cu-ZrO_2 interface in the hollow structure, as shown in Figure 15b, which delivered the best performance for CO_2 hydrogenation to CH_3OH with 5% CO_2 conversion and 85% CH_3OH selectivity at a reaction temperature of 220 °C [197]. Similarly, Yu et al. prepared highly dispersed Cu NPs on ZrO_2 via the calcination and reduction of ZrO_2@HKUST-1 (Figure 15c). Due to the confinement of MOFs, highly dispersed Cu on ZrO_2 was generated, which increased the efficient active sites and produced more interface between the Cu and ZrO_2. The as-prepared catalysts exhibited 5.2 times higher CH_3OH yield than that of those catalysts prepared by the conventional impregnation method [198]. Similar enhancement was also demonstrated in the PdZn alloy and In_2O_3/Pd during CO_2 hydrogenation [199,200].
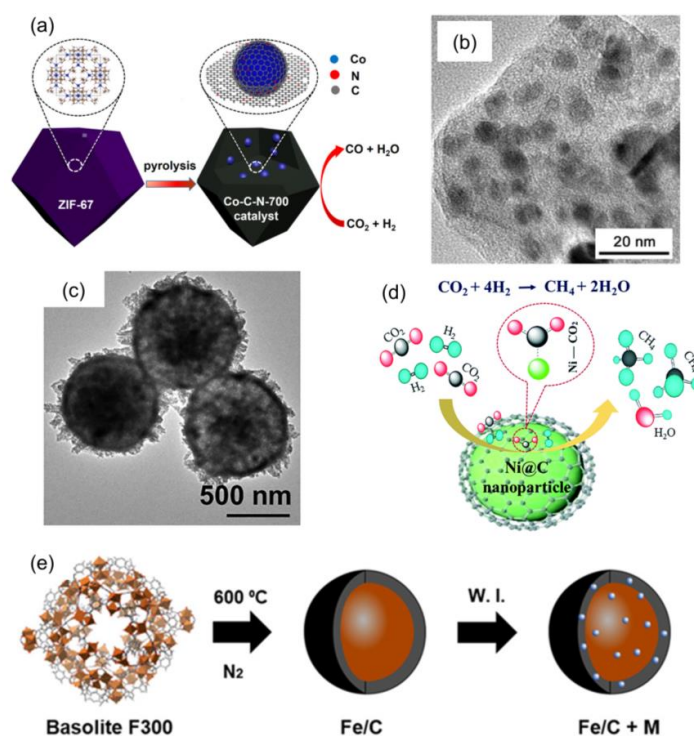
Figure 14. (**a**) The scheme of cobalt-based nonprecious metal catalysts derived from MOFs for selective CO_2 hydrogenation to CO. (**b**) TEM image of Co-C-N-700 catalyst. Reproduced with permission [161]. Copyright 2019, American Chemical Society. (**c**) TEM image of the hierarchical Ni@C hollow spheres. (**d**) The scheme of Ni-based nonprecious metal catalysts derived from MOFs for selective CO_2 hydrogenation to CH_4. Reproduced with permission [168]. Copyright 2019, Royal Society of Chemistry. (**e**) The scheme of the preparation of the Fe-based catalyst. Reproduced with permission [56]. Copyright 2018, American Chemical Society.
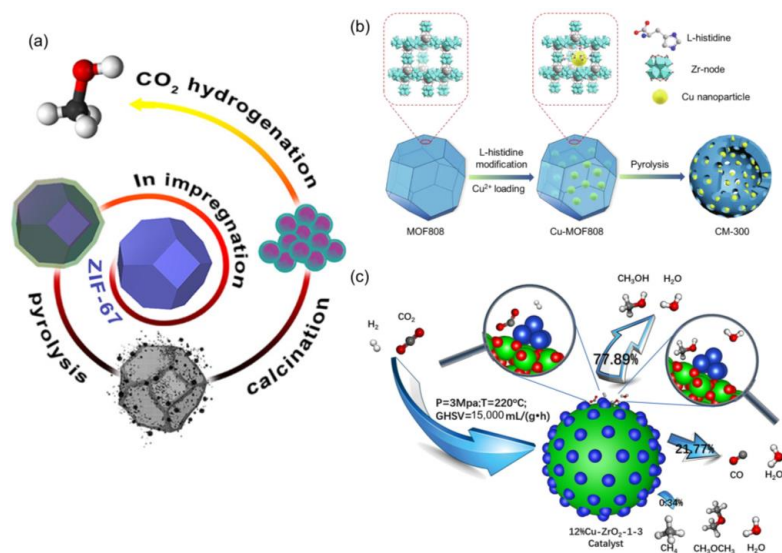

Figure 15. (**a**) The scheme of MOF-derived synthesis of CoIn-based catalysts for CO_2 hydrogenation. Reproduced with permission [191]. Copyright 2018, American Chemical Society. (**b**) The scheme of catalysts preparation for Cu^+-ZrO_2 interfacial sites with highly dispersed copper NPs derived from Cu@UiO-67. Reproduced with permission [197]. Copyright 2018, Elsevier. (**c**) The scheme of highly dispersed Cu NPs on ZrO_2 derived from ZrO_2@ HKUST-1 composites for CO_2 hydrogenation to CH_3OH. Reproduced with permission [198]. Copyright 2021, Elsevier.

Overall, the MOF-derived materials exhibited higher stability than MOFs themselves in CO_2 hydrogenation. The electronic effects of SMSI and interfacial catalysis could dramatically enhance catalytic performance. However, the reaction mechanism at the molecular level remains elusive; more advanced operando characterizations in conjunction with theoretical calculation are needed in further work to decipher the mechanism in greater detail. It is worth noting that the encapsulating layer (especially the carbon layer) seems to be consumed on stream to decrease the catalytic performance because of the involvement in CO_2 hydrogenation.

4. Conclusions and Outlook

Different from zeolite with fixed tetrahedral Si/Al coordination and pore sizes (<1 nm) [201], the uniform and tunable cavities and tailorable composite make MOFs especially attractive for heterogeneous catalysis. The confinement effects in MOFs or MOF-derived materials involving immobilization, size of active sites, encapsulation, and synergy effect significantly perturb the catalytic performance of CO_2 hydrogenation. In this review, the microstructural optimization and engineering of MOF-based catalysts for CO_2 hydrogenation were systematically summarized. The MOFs or MOF-derived catalysts can be simply divided into three categories: (1) molecular complexes, atomic or nanosized active species are confined into cavities or channels of MOFs via one-pot synthesis or post-synthetic modification; (2) active species are surrounded by MOFs or MOF membranes by epitaxial growth; (3) active sites are embedded in carbon or oxide layers derived from MOFs. The most important merits of the heterogenized molecular complexes are their dramatically enhanced recyclability and stability. The advantages of the confined NPs are the cage or channel stabilization and modification of the local reaction microenvironment. The composites derived from MOFs exhibited strong electronic transfer effects and increased interface catalysis between active sites and the encapsulating layers.

Despite all the progress achieved by researchers, many problems remain unsolved. For example, the precise synthesis with desired spatial distribution, loading, and size of active species in MOFs represent the biggest challenges in this field; the hydrothermal stability of host MOFs under reaction conditions is still limited; most products are CO, CH_4, and CH_3OH, but the high-value-added chemicals or fuels produced from CO_2 hydrogenation are limited; and the enhancement interpretation of confinement effects at the molecular level is less than well understood.

In the future, extensive efforts are required to resolve the existing challenges. The detailed directions are as follows:

1. The development of sophisticated organic synthesis to design more linkers with desired functional groups is highly needed, which will make the precise tailoring of active sites highly possible. For example, some functional groups (e.g., carboxyl, sulfonic acid, or amino groups) are effective to stabilize the active sites; therefore, their controllable synthesis with desired positions and contents are essential to obtain rationally designed catalysts.

2. More fundamental interpretations for MOF nucleation, growth, decomposition, and collapsing can provide a strong foundation for more stable MOFs preparations. Since the generated water in CO_2 hydrogenation is unavoidable, water management near the active sites can change the stability of MOFs and tune product distributions.

3. To date, only imidazole or carboxylate-based MOFs were widely investigated for CO_2 hydrogenation; more linkers and metal nodes (e.g., Ru, Ti, Mo, and Mn) are needed to obtain a higher diversity of applicable MOFs. Apart from Cu-, Zr-, or Zn-based composites, some new catalyst systems (e.g., Ru, Mn, and Rh) are more interesting for high-value-added chemicals or fuel formation.

4. Advanced characterization techniques are required to reveal the structure of the active sites; the reaction mechanisms at the molecular scale are helpful to increase the selectivity of target products.

References

1. Li, X.; Liu, G.; Xu, D.; Hong, X.; Edman Tsang, S.C. Confinement of subnanometric PdZn at a defect enriched ZnO/ZIF-8 interface for efficient and selective CO_2 hydrogenation to methanol. *J. Mater. Chem. A* **2019**, *7*, 23878–23885. [CrossRef]
2. Lu, X.; Ahsaine, H.A.; Dereli, B.; Garcia-Esparza, A.T.; Reinhard, M.; Shinagawa, T.; Li, D.; Adil, K.; Tchalala, M.R.; Kroll, T.; et al. Operando Elucidation on the Working State of Immobilized Fluorinated Iron Porphyrin for Selective Aqueous Electroreduction of CO_2 to CO. *ACS Catal.* **2021**, *11*, 6499–6509. [CrossRef]
3. Gao, P.; Zhang, L.; Li, S.; Zhou, Z.; Sun, Y. Novel heterogeneous catalysts for CO_2 hydrogenation to liquid fuels. *ACS Cent. Sci.* **2020**, *6*, 1657–1670. [CrossRef] [PubMed]
4. Lu, X.; Dereli, B.; Shinagawa, T.; Eddaoudi, M.; Cavallo, L.; Takanabe, K. High current density microkinetic and electronic structure analysis of CO_2 reduction using Co and Fe complexes on gas diffusion electrode. *Chem Catal.* **2022**, *2*, 1143–1162. [CrossRef]
5. He, Z.; Cui, M.; Qian, Q.; Zhang, J.; Liu, H.; Han, B. Synthesis of liquid fuel via direct hydrogenation of CO_2. *Proc. Natl. Acad. Sci. USA* **2019**, *116*, 12654–12659. [CrossRef]
6. Jiang, X.; Nie, X.; Guo, X.; Song, C.; Chen, J.G. Recent Advances in Carbon Dioxide Hydrogenation to Methanol via Heterogeneous Catalysis. *Chem. Rev.* **2020**, *120*, 7984–8034. [CrossRef]
7. Zeng, F.; Mebrahtu, C.; Xi, X.; Liao, L.; Ren, J.; Xie, J.; Heeres, H.J.; Palkovits, R. Catalysts design for higher alcohols synthesis by CO_2 hydrogenation: Trends and future perspectives. *Appl. Catal. B Environ.* **2021**, *291*, 120073. [CrossRef]
8. Juneau, M.; Liu, R.; Peng, Y.; Malge, A.; Ma, Z.; Porosoff, M.D. Characterization of Metal-zeolite Composite Catalysts: Determining the Environment of the Active Phase. *ChemCatChem* **2020**, *12*, 1826–1852. [CrossRef]
9. Goud, D.; Gupta, R.; Maligal-Ganesh, R.; Peter, S.C. Review of catalyst design and mechanistic studies for the production of olefins from anthropogenic CO_2. *ACS Catal.* **2020**, *10*, 14258–14282. [CrossRef]
10. Wang, J.; Li, G.; Li, Z.; Tang, C.; Feng, Z.; An, H.; Liu, H.; Liu, T.; Li, C. A highly selective and stable $ZnO-ZrO_2$ solid solution catalyst for CO2 hydrogenation to methanol. *Sci. Adv.* **2017**, *3*, e1701290. [CrossRef]
11. Wei, J.; Ge, Q.; Yao, R.; Wen, Z.; Fang, C.; Guo, L.; Xu, H.; Sun, J. Directly converting CO_2 into a gasoline fuel. *Nat. Commun.* **2017**, *8*, 15174. [CrossRef]
12. Guo, L.; Sun, J.; Ge, Q.; Tsubaki, N. Recent advances in direct catalytic hydrogenation of carbon dioxide to valuable C_{2+} hydrocarbons. *J. Mater. Chem. A* **2018**, *6*, 23244–23262. [CrossRef]
13. Han, Y.; Fang, C.; Ji, X.; Wei, J.; Ge, Q.; Sun, J. Interfacing with carbonaceous potassium promoters boosts catalytic CO_2 hydrogenation of iron. *ACS Catal.* **2020**, *10*, 12098–12108. [CrossRef]
14. Yao, R.; Wei, J.; Ge, Q.; Xu, J.; Han, Y.; Ma, Q.; Xu, H.; Sun, J. Monometallic iron catalysts with synergistic Na and S for higher alcohols synthesis via CO_2 hydrogenation. *Appl. Catal. B Environ.* **2021**, *298*, 120556. [CrossRef]
15. Cheng, K.; Gu, B.; Liu, X.; Kang, J.; Zhang, Q.; Wang, Y. Direct and Highly Selective Conversion of Synthesis Gas into Lower Olefins: Design of a Bifunctional Catalyst Combining Methanol Synthesis and Carbon–Carbon Coupling. *Angew. Chem. Int. Ed.* **2016**, *55*, 4725–4728. [CrossRef] [PubMed]
16. Fujiwara, M.; Souma, Y. Hydrocarbon synthesis from carbon dioxide and hydrogen over Cu–Zn–Cr oxide/zeolite hybrid catalysts. *J. Chem. Soc. Chem. Commun.* **1992**, *10*, 767–768. [CrossRef]
17. Park, Y.-K.; Park, K.-C.; Ihm, S.-K. Hydrocarbon synthesis through CO_2 hydrogenation over $CuZnOZrO_2$/zeolite hybrid catalysts. *Catal. Today* **1998**, *44*, 165–173. [CrossRef]
18. Kunkes, E.L.; Studt, F.; Abild-Pedersen, F.; Schlögl, R.; Behrens, M. Hydrogenation of CO_2 to methanol and CO on $Cu/ZnO/Al_2O_3$: Is there a common intermediate or not? *J. Catal.* **2015**, *328*, 43–48. [CrossRef]
19. Lunkenbein, T.; Schumann, J.; Behrens, M.; Schlögl, R.; Willinger, M.G. Formation of a ZnO Overlayer in Industrial $Cu/ZnO/Al_2O_3$ Catalysts Induced by Strong Metal–Support Interactions. *Angew. Chem. Int. Ed.* **2015**, *54*, 4544–4548. [CrossRef]
20. Palomino, R.M.; Ramírez, P.J.; Liu, Z.; Hamlyn, R.; Waluyo, I.; Mahapatra, M.; Orozco, I.; Hunt, A.; Simonovis, J.P.; Senanayake, S.D.; et al. Hydrogenation of CO_2 on ZnO/Cu(100) and ZnO/Cu(111) Catalysts: Role of Copper Structure and Metal–Oxide Interface in Methanol Synthesis. *J. Phys. Chem. B* **2018**, *122*, 794–800. [CrossRef]
21. Sun, Y.; Xia, Y. Shape-controlled synthesis of gold and silver nanoparticles. *Science* **2002**, *298*, 2176–2179. [CrossRef] [PubMed]

22. Shi, Y.; Lyu, Z.; Zhao, M.; Chen, R.; Nguyen, Q.N.; Xia, Y. Noble-metal nanocrystals with controlled shapes for catalytic and electrocatalytic applications. *Chem. Rev.* **2020**, *121*, 649–735. [CrossRef] [PubMed]

23. Dai, Y.; Lu, P.; Cao, Z.; Campbell, C.T.; Xia, Y. The physical chemistry and materials science behind sinter-resistant catalysts. *Chem. Soc. Rev.* **2018**, *47*, 4314–4331. [CrossRef] [PubMed]

24. Wu, C.; Lin, L.; Liu, J.; Zhang, J.; Zhang, F.; Zhou, T.; Rui, N.; Yao, S.; Deng, Y.; Yang, F.; et al. Inverse ZrO_2/Cu as a highly efficient methanol synthesis catalyst from CO_2 hydrogenation. *Nat. Commun.* **2020**, *11*, 5767. [CrossRef]

25. Lin, L.; Gerlak, C.A.; Liu, C.; Llorca, J.; Yao, S.; Rui, N.; Zhang, F.; Liu, Z.; Zhang, S.; Deng, K.; et al. Effect of Ni particle size on the production of renewable methane from CO_2 over Ni/CeO_2 catalyst. *J. Energy Chem.* **2021**, *61*, 602–611. [CrossRef]

26. Liu, R.; Leshchev, D.; Stavitski, E.; Juneau, M.; Agwara, J.N.; Porosoff, M.D. Selective hydrogenation of CO_2 and CO over potassium promoted Co/ZSM-5. *Appl. Catal. B Environ.* **2021**, *284*, 119787. [CrossRef]

27. Meng, G.; Sun, J.; Tao, L.; Ji, K.; Wang, P.; Wang, Y.; Sun, X.; Cui, T.; Du, S.; Chen, J. Ru_1Co_n Single-Atom Alloy for Enhancing Fischer–Tropsch Synthesis. *ACS Catal.* **2021**, *11*, 1886–1896. [CrossRef]

28. Zamani, A.H.; Shohaimi, N.A.M.; Rosid, S.J.M.; Abdullah, N.H.; Shukri, N.M. Enhanced low temperature reaction for the CO_2 methanation over Ru promoted Cu/Mn on alumina support catalyst using double reactor system. *J. Taiwan Inst. Chem. Eng.* **2019**, *96*, 400–408. [CrossRef]

29. Wolf, A.; Jess, A.; Kern, C. Syngas Production via Reverse Water-Gas Shift Reaction over a Ni-Al_2O_3 Catalyst: Catalyst Stability, Reaction Kinetics, and Modeling. *Chem. Eng. Tech.* **2016**, *39*, 1040–1048. [CrossRef]

30. Álvarez Galván, C.; Schumann, J.; Behrens, M.; Fierro, J.L.G.; Schlögl, R.; Frei, E. Reverse water-gas shift reaction at the Cu/ZnO interface: Influence of the Cu/Zn ratio on structure-activity correlations. *Appl. Catal. B Environ.* **2016**, *195*, 104–111. [CrossRef]

31. Fichtl, M.B.; Schlereth, D.; Jacobsen, N.; Kasatkin, I.; Schumann, J.; Behrens, M.; Schlögl, R.; Hinrichsen, O. Kinetics of deactivation on Cu/ZnO/Al_2O_3 methanol synthesis catalysts. *Appl. Catal. A Gen.* **2015**, *502*, 262–270. [CrossRef]

32. Weigel, J.; Koeppel, R.A.; Baiker, A.; Wokaun, A. Surface Species in CO and CO_2 Hydrogenation over Copper/Zirconia: On the Methanol Synthesis Mechanism. *Langmuir* **1996**, *12*, 5319–5329. [CrossRef]

33. Lin, L.; Liu, J.; Liu, X.; Gao, Z.; Rui, N.; Yao, S.; Zhang, F.; Wang, M.; Liu, C.; Han, L. Reversing sintering effect of Ni particles on γ-Mo_2N via strong metal support interaction. *Nat. Commun.* **2021**, *12*, 6978. [CrossRef] [PubMed]

34. Zhang, X.; Zhu, X.; Lin, L.; Yao, S.; Zhang, M.; Liu, X.; Wang, X.; Li, Y.-W.; Shi, C.; Ma, D. Highly Dispersed Copper over β-Mo_2C as an Efficient and Stable Catalyst for the Reverse Water Gas Shift (RWGS) Reaction. *ACS Catal.* **2017**, *7*, 912–918. [CrossRef]

35. Li, S.; Xu, Y.; Chen, Y.; Li, W.; Lin, L.; Li, M.; Deng, Y.; Wang, X.; Ge, B.; Yang, C.; et al. Tuning the Selectivity of Catalytic Carbon Dioxide Hydrogenation over Iridium/Cerium Oxide Catalysts with a Strong Metal–Support Interaction. *Angew. Chem. Int. Ed.* **2017**, *56*, 10761–10765. [CrossRef]

36. Wang, H.; Wang, L.; Xiao, F.-S. Metal@Zeolite Hybrid Materials for Catalysis. *ACS Cent. Sci.* **2020**, *6*, 1685–1697. [CrossRef]

37. Zhang, J.; Wang, L.; Zhang, B.; Zhao, H.; Kolb, U.; Zhu, Y.; Liu, L.; Han, Y.; Wang, G.; Wang, C.; et al. Sinter-resistant metal nanoparticle catalysts achieved by immobilization within zeolite crystals via seed-directed growth. *Nat. Catal.* **2018**, *1*, 540–546. [CrossRef]

38. Wang, Y.; Wang, C.; Wang, L.; Wang, L.; Xiao, F.-S. Zeolite fixed metal nanoparticles: New perspective in catalysis. *Acc. Chem. Res.* **2021**, *54*, 2579–2590. [CrossRef]

39. Yang, Z.; Li, H.; Zhou, H.; Wang, L.; Wang, L.; Zhu, Q.; Xiao, J.; Meng, X.; Chen, J.; Xiao, F.-S. Coking-resistant iron catalyst in ethane dehydrogenation achieved through siliceous zeolite modulation. *J. Am. Chem. Soc.* **2020**, *142*, 16429–16436. [CrossRef]

40. Wang, C.; Guan, E.; Wang, L.; Chu, X.; Wu, Z.; Zhang, J.; Yang, Z.; Jiang, Y.; Zhang, L.; Meng, X.; et al. Product Selectivity Controlled by Nanoporous Environments in Zeolite Crystals Enveloping Rhodium Nanoparticle Catalysts for CO_2 Hydrogenation. *J. Am. Chem. Soc.* **2019**, *141*, 8482–8488. [CrossRef]

41. Freund, R.; Zaremba, O.; Arnauts, G.; Ameloot, R.; Skorupskii, G.; Dincă, M.; Bavykina, A.; Gascon, J.; Ejsmont, A.; Goscianska, J.; et al. The Current Status of MOF and COF Applications. *Angew. Chem. Int. Ed.* **2021**, *60*, 23975–24001. [CrossRef] [PubMed]

42. Yalcin, G.; Kayan, A. Synthesis and characterization of Zr, Ti, Al-phthalate and pyridine-2-carboxylate compounds and their use in ring opening polymerization. *Appl. Catal. A Gen.* **2012**, *433*, 223–228. [CrossRef]

43. Ding, M.; Cai, X.; Jiang, H.-L. Improving MOF stability: Approaches and applications. *Chem. Sci.* **2019**, *10*, 10209–10230. [CrossRef] [PubMed]

44. Rubio-Martinez, M.; Avci-Camur, C.; Thornton, A.W.; Imaz, I.; Maspoch, D.; Hill, M.R. New synthetic routes towards MOF production at scale. *Chem. Soc. Rev.* **2017**, *46*, 3453–3480. [CrossRef]

45. Wang, Q.; Astruc, D. State of the art and prospects in metal–organic framework (MOF)-based and MOF-derived nanocatalysis. *Chem. Rev.* **2019**, *120*, 1438–1511. [CrossRef]

46. Lee, J.; Farha, O.K.; Roberts, J.; Scheidt, K.A.; Nguyen, S.T.; Hupp, J.T. Metal–organic framework materials as catalysts. *Chem. Soc. Rev.* **2009**, *38*, 1450–1459. [CrossRef]

47. Huang, Y.-B.; Liang, J.; Wang, X.-S.; Cao, R. Multifunctional metal–organic framework catalysts: Synergistic catalysis and tandem reactions. *Chem. Soc. Rev.* **2017**, *46*, 126–157. [CrossRef]

48. Li, Z.; Rayder, T.M.; Luo, L.; Byers, J.A.; Tsung, C.-K. Aperture-Opening Encapsulation of a Transition Metal Catalyst in a Metal–Organic Framework for CO2 Hydrogenation. *J. Am. Chem. Soc.* **2018**, *140*, 8082–8085. [CrossRef]

49. Liao, F.-S.; Lo, W.-S.; Hsu, Y.-S.; Wu, C.-C.; Wang, S.-C.; Shieh, F.-K.; Morabito, J.V.; Chou, L.-Y.; Wu, K.C.W.; Tsung, C.-K. Shielding against Unfolding by Embedding Enzymes in Metal–Organic Frameworks via a de Novo Approach. *J. Am. Chem. Soc.* **2017**, *139*, 6530–6533. [CrossRef]

50. Morabito, J.V.; Chou, L.-Y.; Li, Z.; Manna, C.M.; Petroff, C.A.; Kyada, R.J.; Palomba, J.M.; Byers, J.A.; Tsung, C.-K. Molecular Encapsulation beyond the Aperture Size Limit through Dissociative Linker Exchange in Metal–Organic Framework Crystals. *J. Am. Chem. Soc.* **2014**, *136*, 12540–12543. [CrossRef]

51. Rayder, T.M.; Adillon, E.H.; Byers, J.A.; Tsung, C.-K. A Bioinspired Multicomponent Catalytic System for Converting Carbon Dioxide into Methanol Autocatalytically. *Chem* **2020**, *6*, 1742–1754. [CrossRef]

52. Rayder, T.M.; Bensalah, A.T.; Li, B.; Byers, J.A.; Tsung, C.-K. Engineering Second Sphere Interactions in a Host–Guest Multicomponent Catalyst System for the Hydrogenation of Carbon Dioxide to Methanol. *J. Am. Chem. Soc.* **2021**, *143*, 1630–1640. [CrossRef] [PubMed]

53. Indra, A.; Song, T.; Paik, U. Metal organic framework derived materials: Progress and prospects for the energy conversion and storage. *Adv. Mater.* **2018**, *30*, 1705146. [CrossRef] [PubMed]

54. Wu, H.B.; Lou, X.W. Metal-organic frameworks and their derived materials for electrochemical energy storage and conversion: Promises and challenges. *Sci. Adv.* **2017**, *3*, eaap9252. [CrossRef]

55. Wang, C.; Kim, J.; Tang, J.; Kim, M.; Lim, H.; Malgras, V.; You, J.; Xu, Q.; Li, J.; Yamauchi, Y. New strategies for novel MOF-derived carbon materials based on nanoarchitectures. *Chem* **2020**, *6*, 19–40. [CrossRef]

56. Ramirez, A.; Gevers, L.; Bavykina, A.; Ould-Chikh, S.; Gascon, J. Metal Organic Framework-Derived Iron Catalysts for the Direct Hydrogenation of CO_2 to Short Chain Olefins. *ACS Catal.* **2018**, *8*, 9174–9182. [CrossRef]

57. Sajitha, E.P.; Prasad, V.; Subramanyam, S.V.; Eto, S.; Takai, K.; Enoki, T. Synthesis and characteristics of iron nanoparticles in a carbon matrix along with the catalytic graphitization of amorphous carbon. *Carbon* **2004**, *42*, 2815–2820. [CrossRef]

58. Zhu, J.; Zhang, G.; Li, W.; Zhang, X.; Ding, F.; Song, C.; Guo, X. Deconvolution of the particle size effect on CO_2 hydrogenation over iron-based catalysts. *ACS Catal.* **2020**, *10*, 7424–7433. [CrossRef]

59. Wu, S.-M.; Yang, X.-Y.; Janiak, C. Confinement Effects in Zeolite-Confined Noble Metals. *Angew. Chem. Int. Ed.* **2019**, *58*, 12340–12354. [CrossRef]

60. Shao, S.; Cui, C.; Tang, Z.; Li, G. Recent advances in metal-organic frameworks for catalytic CO_2 hydrogenation to diverse products. *Nano Res.* **2022**, *15*, 10110–10133. [CrossRef]

61. Li, G.; Zhao, S.; Zhang, Y.; Tang, Z. Metal–Organic Frameworks Encapsulating Active Nanoparticles as Emerging Composites for Catalysis: Recent Progress and Perspectives. *Adv. Mater.* **2018**, *30*, 1800702. [CrossRef]

62. Howarth, A.J.; Peters, A.W.; Vermeulen, N.A.; Wang, T.C.; Hupp, J.T.; Farha, O.K. Best Practices for the Synthesis, Activation, and Characterization of Metal–Organic Frameworks. *Chem. Mater.* **2017**, *29*, 26–39. [CrossRef]

63. Stock, N.; Biswas, S. Synthesis of metal-organic frameworks (MOFs): Routes to various MOF topologies, morphologies, and composites. *Chem. Rev.* **2012**, *112*, 933–969. [CrossRef] [PubMed]

64. Li, Y.-N.; Ma, R.; He, L.-N.; Diao, Z.-F. Homogeneous hydrogenation of carbon dioxide to methanol. *Catal. Sci. Techol.* **2014**, *4*, 1498–1512. [CrossRef]

65. Yoshio, I.; Hitoshi, I.; Yoshiyuki, S.; Harukichi, H. Catalytic Fixation of Carbon Dioxide to Formic Acid by Transition-Metal Complexes Under Mild Conditions. *Chem. Lett.* **1976**, *5*, 863–864.

66. Tanaka, R.; Yamashita, M.; Nozaki, K. Catalytic Hydrogenation of Carbon Dioxide Using Ir(III)−Pincer Complexes. *J. Am. Chem. Soc.* **2009**, *131*, 14168–14169. [CrossRef] [PubMed]

67. Sanz, S.; Azua, A.; Peris, E. '(η6-arene)Ru(bis-NHC)' complexes for the reduction of CO_2 to formate with hydrogen and by transfer hydrogenation with iPrOH. *Dalton Trans.* **2010**, *39*, 6339–6343. [CrossRef]

68. Sanz, S.; Benítez, M.; Peris, E. A New Approach to the Reduction of Carbon Dioxide: CO_2 Reduction to Formate by Transfer Hydrogenation in iPrOH. *Organometallics* **2010**, *29*, 275–277. [CrossRef]

69. Azua, A.; Sanz, S.; Peris, E. Water-Soluble IrIII N-Heterocyclic Carbene Based Catalysts for the Reduction of CO_2 to Formate by Transfer Hydrogenation and the Deuteration of Aryl Amines in Water. *Chem.–Eur. J.* **2011**, *17*, 3963–3967. [CrossRef]

70. Filonenko, G.A.; van Putten, R.; Schulpen, E.N.; Hensen, E.J.M.; Pidko, E.A. Highly Efficient Reversible Hydrogenation of Carbon Dioxide to Formates Using a Ruthenium PNP-Pincer Catalyst. *ChemCatChem* **2014**, *6*, 1526–1530. [CrossRef]

71. Gunasekar, G.H.; Park, K.; Jung, K.-D.; Yoon, S. Recent developments in the catalytic hydrogenation of CO_2 to formic acid/formate using heterogeneous catalysts. *Inorg. Chem. Front.* **2016**, *3*, 882–895. [CrossRef]

72. Álvarez, A.; Bansode, A.; Urakawa, A.; Bavykina, A.V.; Wezendonk, T.A.; Makkee, M.; Gascon, J.; Kapteijn, F. Challenges in the Greener Production of Formates/Formic Acid, Methanol, and DME by Heterogeneously Catalyzed CO_2 Hydrogenation Processes. *Chem. Rev.* **2017**, *117*, 9804–9838. [CrossRef] [PubMed]

73. Wu, C.; Irshad, F.; Luo, M.; Zhao, Y.; Ma, X.; Wang, S. Ruthenium Complexes Immobilized on an Azolium Based Metal Organic Framework for Highly Efficient Conversion of CO_2 into Formic Acid. *ChemCatChem* **2019**, *11*, 1256–1263. [CrossRef]

74. Gadzikwa, T.; Farha, O.K.; Mulfort, K.L.; Hupp, J.T.; Nguyen, S.T. A Zn-based, pillared paddlewheel MOF containing free carboxylic acids via covalent post-synthesis elaboration. *Chem. Commun.* **2009**, 3720–3722. [CrossRef]

75. Li, B.; Zhang, Y.; Ma, D.; Ma, T.; Shi, Z.; Ma, S. Metal-Cation-Directed de Novo Assembly of a Functionalized Guest Molecule in the Nanospace of a Metal–Organic Framework. *J. Am. Chem. Soc.* **2014**, *136*, 1202–1205. [CrossRef]

76. Chen, J.; Gong, X.; Li, J.; Li, Y.; Ma, J.; Hou, C.; Zhao, G.; Yuan, W.; Zhao, B. Carbonyl catalysis enables a biomimetic asymmetric Mannich reaction. *Science* **2018**, *360*, 1438–1442. [CrossRef]

77. Helm, M.L.; Stewart, M.P.; Bullock, R.M.; DuBois, M.R.; DuBois, D.L. A Synthetic Nickel Electrocatalyst with a Turnover Frequency Above 100,000 for H$_2$ Production. *Science* **2011**, *333*, 863–866. [CrossRef]

78. Cirujano, F.G.; Corma, A.; Llabrés i Xamena, F.X. Conversion of levulinic acid into chemicals: Synthesis of biomass derived levulinate esters over Zr-containing MOFs. *Chem. Eng. Sci.* **2015**, *124*, 52–60. [CrossRef]

79. Huff, C.A.; Sanford, M.S. Cascade Catalysis for the Homogeneous Hydrogenation of CO$_2$ to Methanol. *J. Am. Chem. Soc.* **2011**, *133*, 18122–18125. [CrossRef]

80. Martínez Cuesta, S.; Rahman, S.A.; Furnham, N.; Thornton, J.M. The Classification and Evolution of Enzyme Function. *Biophys. J.* **2015**, *109*, 1082–1086. [CrossRef]

81. Li, Z.; Wang, D.; Wu, Y.; Li, Y. Recent advances in the precise control of isolated single-site catalysts by chemical methods. *Nat. Sci. Rev.* **2018**, *5*, 673–689. [CrossRef]

82. Liu, X.-M.; Lu, G.Q.; Yan, Z.-F.; Beltramini, J. Recent Advances in Catalysts for Methanol Synthesis via Hydrogenation of CO and CO$_2$. *Ind. Eng. Chem. Res.* **2003**, *42*, 6518–6530. [CrossRef]

83. Valdés, H.; García-Eleno, M.A.; Canseco-Gonzalez, D.; Morales-Morales, D. Recent Advances in Catalysis with Transition-Metal Pincer Compounds. *ChemCatChem* **2018**, *10*, 3136–3172. [CrossRef]

84. Trost, B.M.; Bunt, R.C. On Ligand Design for Catalytic Outer Sphere Reactions: A Simple Asymmetric Synthesis of Vinylglycinol. *Angew. Chem. Int. Ed.* **1996**, *35*, 99–102. [CrossRef]

85. Carboni, S.; Gennari, C.; Pignataro, L.; Piarulli, U. Supramolecular ligand–ligand and ligand–substrate interactions for highly selective transition metal catalysis. *Dalton Trans.* **2011**, *40*, 4355–4373. [CrossRef]

86. Prokopchuk, D.E.; Morris, R.H. Inner-Sphere Activation, Outer-Sphere Catalysis: Theoretical Study on the Mechanism of Transfer Hydrogenation of Ketones Using Iron(II) PNNP Eneamido Complexes. *Organometallics* **2012**, *31*, 7375–7385. [CrossRef]

87. Allendorf, M.D.; Foster, M.E.; Léonard, F.; Stavila, V.; Feng, P.L.; Doty, F.P.; Leong, K.; Ma, E.Y.; Johnston, S.R.; Talin, A.A. Guest-Induced Emergent Properties in Metal–Organic Frameworks. *J. Phys. Chem. Lett.* **2015**, *6*, 1182–1195. [CrossRef]

88. Sharp, C.H.; Bukowski, B.C.; Li, H.; Johnson, E.M.; Ilic, S.; Morris, A.J.; Gersappe, D.; Snurr, R.Q.; Morris, J.R. Nanoconfinement and mass transport in metal–organic frameworks. *Chem. Soc. Rev.* **2021**, *50*, 11530–11558. [CrossRef]

89. Tong, P.-H.; Zhu, L.; Zang, Y.; Li, J.; He, X.-P.; James, T.D. Metal–organic frameworks (MOFs) as host materials for the enhanced delivery of biomacromolecular therapeutics. *Chem. Commun.* **2021**, *57*, 12098–12110. [CrossRef]

90. Zhang, X.; Tu, R.; Lu, Z.; Peng, J.; Hou, C.; Wang, Z. Hierarchical mesoporous metal–organic frameworks encapsulated enzymes: Progress and perspective. *Coord. Chem. Rev.* **2021**, *443*, 214032. [CrossRef]

91. Alkordi, M.H.; Liu, Y.; Larsen, R.W.; Eubank, J.F.; Eddaoudi, M. Zeolite-like Metal−Organic Frameworks as Platforms for Applications: On Metalloporphyrin-Based Catalysts. *J. Am. Chem. Soc.* **2008**, *130*, 12639–12641. [CrossRef] [PubMed]

92. Larsen, R.W.; Wojtas, L. Photoinduced inter-cavity electron transfer between Ru(ii)tris(2,2′-bipyridne) and Co(ii)tris(2,2′-bipyridine) Co-encapsulated within a Zn(ii)-trimesic acid metal organic framework. *J. Mater. Chem. A* **2013**, *1*, 14133–14139. [CrossRef]

93. Øien, S.; Agostini, G.; Svelle, S.; Borfecchia, E.; Lomachenko, K.A.; Mino, L.; Gallo, E.; Bordiga, S.; Olsbye, U.; Lillerud, K.P.; et al. Probing Reactive Platinum Sites in UiO-67 Zirconium Metal–Organic Frameworks. *Chem. Mater.* **2015**, *27*, 1042–1056. [CrossRef]

94. An, B.; Zeng, L.; Jia, M.; Li, Z.; Lin, Z.; Song, Y.; Zhou, Y.; Cheng, J.; Wang, C.; Lin, W. Molecular Iridium Complexes in Metal–Organic Frameworks Catalyze CO$_2$ Hydrogenation via Concerted Proton and Hydride Transfer. *J. Am. Chem. Soc.* **2017**, *139*, 17747–17750. [CrossRef] [PubMed]

95. Tshuma, P.; Makhubela, B.C.E.; Bingwa, N.; Mehlana, G. Palladium(II) Immobilized on Metal–Organic Frameworks for Catalytic Conversion of Carbon Dioxide to Formate. *Inorg. Chem.* **2020**, *59*, 6717–6728. [CrossRef]

96. Wang, S.; Hou, S.; Wu, C.; Zhao, Y.; Ma, X. RuCl$_3$ anchored onto post-synthetic modification MIL-101(Cr)-NH2 as heterogeneous catalyst for hydrogenation of CO$_2$ to formic acid. *Chin. Chem. Lett.* **2019**, *30*, 398–402. [CrossRef]

97. Hu, X.; Luo, M.; ur Rehman, M.; Sun, J.; Yaseen, H.A.S.M.; Irshad, F.; Zhao, Y.; Wang, S.; Ma, X. Mechanistic insight into the electron-donation effect of modified ZIF-8 on Ru for CO2 hydrogenation to formic acid. *J. CO2 Util.* **2022**, *60*, 101992. [CrossRef]

98. Ye, R.-P.; Ding, J.; Gong, W.; Argyle, M.D.; Zhong, Q.; Wang, Y.; Russell, C.K.; Xu, Z.; Russell, A.G.; Li, Q. CO$_2$ hydrogenation to high-value products via heterogeneous catalysis. *Nat. Commun.* **2019**, *10*, 5698. [CrossRef]

99. Xu, D.; Wang, Y.; Ding, M.; Hong, X.; Liu, G.; Tsang, S.C.E. Advances in higher alcohol synthesis from CO$_2$ hydrogenation. *Chem* **2021**, *7*, 849–881. [CrossRef]

100. Zhang, X.; Liu, J.-X.; Zijlstra, B.; Filot, I.A.; Zhou, Z.; Sun, S.; Hensen, E.J. Optimum Cu nanoparticle catalysts for CO$_2$ hydrogenation towards methanol. *Nano Energy* **2018**, *43*, 200–209. [CrossRef]

101. Sun, R.; Liao, Y.; Bai, S.-T.; Zheng, M.; Zhou, C.; Zhang, T.; Sels, B.F. Heterogeneous catalysts for CO$_2$ hydrogenation to formic acid/formate: From nanoscale to single atom. *Energy Environ. Sci.* **2021**, *14*, 1247–1285. [CrossRef]

102. Fletcher, A.J.; Thomas, K.M.; Rosseinsky, M.J. Flexibility in metal-organic framework materials: Impact on sorption properties. *J. Solid State Chem.* **2005**, *178*, 2491–2510. [CrossRef]

103. Costa, J.S.; Gamez, P.; Black, C.A.; Roubeau, O.; Teat, S.J.; Reedijk, J. Chemical Modification of a Bridging Ligand Inside a Metal–Organic Framework while Maintaining the 3D Structure. *Eur. J. Inorg. Chem.* **2008**, *2008*, 1551–1554. [CrossRef]

104. Kim, M.; Cahill, J.F.; Fei, H.; Prather, K.A.; Cohen, S.M. Postsynthetic Ligand and Cation Exchange in Robust Metal–Organic Frameworks. *J. Am. Chem. Soc.* **2012**, *134*, 18082–18088. [CrossRef] [PubMed]

105. Karagiaridi, O.; Lalonde, M.B.; Bury, W.; Sarjeant, A.A.; Farha, O.K.; Hupp, J.T. Opening ZIF-8: A Catalytically Active Zeolitic Imidazolate Framework of Sodalite Topology with Unsubstituted Linkers. *J. Am. Chem. Soc.* **2012**, *134*, 18790–18796. [CrossRef] [PubMed]

106. Shu, X.; Yu, Y.; Jiang, Y.; Luan, Y.; Ramella, D. Direct synthesis of Fe(III) immobilized Zr-based metal–organic framework for aerobic oxidation reaction. *Appl. Organomet. Chem.* **2017**, *31*, e3862. [CrossRef]

107. Ye, J.; Johnson, J.K. Design of Lewis Pair-Functionalized Metal Organic Frameworks for CO_2 Hydrogenation. *ACS Catal.* **2015**, *5*, 2921–2928. [CrossRef]

108. Li, W.; Wang, H.; Jiang, X.; Zhu, J.; Liu, Z.; Guo, X.; Song, C. A short review of recent advances in CO_2 hydrogenation to hydrocarbons over heterogeneous catalysts. *RSC Adv.* **2018**, *8*, 7651–7669. [CrossRef]

109. Lu, W.; Wei, Z.; Gu, Z.-Y.; Liu, T.-F.; Park, J.; Park, J.; Tian, J.; Zhang, M.; Zhang, Q.; Gentle Iii, T.; et al. Tuning the structure and function of metal–organic frameworks via linker design. *Chem. Soc. Rev.* **2014**, *43*, 5561–5593. [CrossRef]

110. Choi, H.; Oh, S.; Trung Tran, S.B.; Park, J.Y. Size-controlled model Ni catalysts on Ga_2O_3 for CO_2 hydrogenation to methanol. *J. Catal.* **2019**, *376*, 68–76. [CrossRef]

111. Jia, X.; Sun, K.; Wang, J.; Shen, C.; Liu, C.-J. Selective hydrogenation of CO_2 to methanol over Ni/In_2O_3 catalyst. *J. Energy Chem.* **2020**, *50*, 409–415. [CrossRef]

112. Zhu, J.; Cannizzaro, F.; Liu, L.; Zhang, H.; Kosinov, N.; Filot, I.A.W.; Rabeah, J.; Brückner, A.; Hensen, E.J.M. Ni–In Synergy in CO_2 Hydrogenation to Methanol. *ACS Catal.* **2021**, *11*, 11371–11384. [CrossRef] [PubMed]

113. Dostagir, N.H.M.D.; Thompson, C.; Kobayashi, H.; Karim, A.M.; Fukuoka, A.; Shrotri, A. Rh promoted In_2O_3 as a highly active catalyst for CO_2 hydrogenation to methanol. *Catal. Sci. Technol.* **2020**, *10*, 8196–8202. [CrossRef]

114. Zhang, Z.; Shen, C.; Sun, K.; Liu, C.-J. Improvement in the activity of Ni/In_2O_3 with the addition of ZrO_2 for CO_2 hydrogenation to methanol. *Catal. Commun.* **2022**, *162*, 106386. [CrossRef]

115. Zhang, H.; Liu, G.; Shi, L.; Ye, J. Single-atom catalysts: Emerging multifunctional materials in heterogeneous catalysis. *Adv. Energy Mater.* **2018**, *8*, 1701343. [CrossRef]

116. Wang, A.; Li, J.; Zhang, T. Heterogeneous single-atom catalysis. *Nat. Rev. Chem.* **2018**, *2*, 65–81. [CrossRef]

117. Beniya, A.; Higashi, S. Towards dense single-atom catalysts for future automotive applications. *Nat. Catal.* **2019**, *2*, 590–602. [CrossRef]

118. Yang, X.-F.; Wang, A.; Qiao, B.; Li, J.; Liu, J.; Zhang, T. Single-atom catalysts: A new frontier in heterogeneous catalysis. *Acc. Chem. Res.* **2013**, *46*, 1740–1748. [CrossRef]

119. Hosseiniamoli, H.; Bryant, G.; Kennedy, E.M.; Mathisen, K.; Nicholson, D.; Sankar, G.; Setiawan, A.; Stockenhuber, M. Understanding Structure–Function Relationships in Zeolite-Supported Pd Catalysts for Oxidation of Ventilation Air Methane. *ACS Catal.* **2018**, *8*, 5852–5863. [CrossRef]

120. Lei, Y.; Mehmood, F.; Lee, S.; Greeley, J.; Lee, B.; Seifert, S.; Winans, R.E.; Elam, J.W.; Meyer, R.J.; Redfern, P.C.; et al. Increased Silver Activity for Direct Propylene Epoxidation via Subnanometer Size Effects. *Science* **2010**, *328*, 224–228. [CrossRef]

121. Zhang, J.; An, B.; Li, Z.; Cao, Y.; Dai, Y.; Wang, W.; Zeng, L.; Lin, W.; Wang, C. Neighboring Zn–Zr Sites in a Metal–Organic Framework for CO_2 Hydrogenation. *J. Am. Chem. Soc.* **2021**, *143*, 8829–8837. [CrossRef] [PubMed]

122. Tian, P.; Zhan, G.; Tian, J.; Tan, K.B.; Guo, M.; Han, Y.; Fu, T.; Huang, J.; Li, Q. Direct CO_2 Hydrogenation to Light Olefins over ZnZrOx Mixed with Hierarchically Hollow SAPO-34 with Rice Husk as Green Silicon Source and Template. *Appl. Catal. B Environ.* **2022**, *315*, 121572. [CrossRef]

123. An, B.; Li, Z.; Song, Y.; Zhang, J.; Zeng, L.; Wang, C.; Lin, W. Cooperative copper centres in a metal–organic framework for selective conversion of CO_2 to ethanol. *Nat. Catal.* **2019**, *2*, 709–717. [CrossRef]

124. Feng, X.; Ji, P.; Li, Z.; Drake, T.; Oliveres, P.; Chen, E.Y.; Song, Y.; Wang, C.; Lin, W. Aluminum Hydroxide Secondary Building Units in a Metal–Organic Framework Support Earth-Abundant Metal Catalysts for Broad-Scope Organic Transformations. *ACS Catal.* **2019**, *9*, 3327–3337. [CrossRef]

125. Feng, X.; Song, Y.; Chen, J.S.; Xu, Z.; Dunn, S.J.; Lin, W. Rational Construction of an Artificial Binuclear Copper Monooxygenase in a Metal–Organic Framework. *J. Am. Chem. Soc.* **2021**, *143*, 1107–1118. [CrossRef]

126. Zeng, L.; Cao, Y.; Li, Z.; Dai, Y.; Wang, Y.; An, B.; Zhang, J.; Li, H.; Zhou, Y.; Lin, W.; et al. Multiple Cuprous Centers Supported on a Titanium-Based Metal–Organic Framework Catalyze CO_2 Hydrogenation to Ethylene. *ACS Catal.* **2021**, *11*, 11696–11705. [CrossRef]

127. Chen, Y.; Li, H.; Zhao, W.; Zhang, W.; Li, J.; Li, W.; Zheng, X.; Yan, W.; Zhang, W.; Zhu, J.; et al. Optimizing reaction paths for methanol synthesis from CO_2 hydrogenation via metal-ligand cooperativity. *Nat. Commun.* **2019**, *10*, 1885. [CrossRef]

128. Matsubu, J.C.; Zhang, S.; DeRita, L.; Marinkovic, N.S.; Chen, J.G.; Graham, G.W.; Pan, X.; Christopher, P. Adsorbate-mediated strong metal–support interactions in oxide-supported Rh catalysts. *Nat. Chem.* **2017**, *9*, 120–127. [CrossRef]

129. Cargnello, M.; Doan-Nguyen, V.V.T.; Gordon, T.R.; Diaz, R.E.; Stach, E.A.; Gorte, R.J.; Fornasiero, P.; Murray, C.B. Control of Metal Nanocrystal Size Reveals Metal-Support Interface Role for Ceria Catalysts. *Science* **2013**, *341*, 771–773. [CrossRef]

130. Wodiunig, S.; Keel, J.M.; Wilson, T.S.E.; Zemichael, F.W.; Lambert, R.M. AFM and XPS Study of the Sintering of Realistic Ag/α-Al_2O_3 Model Catalysts Under Conditions of Ethene Epoxidation. *Catal. Lett.* **2003**, *87*, 1–5. [CrossRef]

131. Tauster, S.J.; Fung, S.C.; Garten, R.L. Strong metal-support interactions. Group 8 noble metals supported on titanium dioxide. *J. Am. Chem. Soc.* **1978**, *100*, 170–175. [CrossRef]

132. Li, Z.; Ji, S.; Liu, Y.; Cao, X.; Tian, S.; Chen, Y.; Niu, Z.; Li, Y. Well-Defined Materials for Heterogeneous Catalysis: From Nanoparticles to Isolated Single-Atom Sites. *Chem. Rev.* **2020**, *120*, 623–682. [CrossRef] [PubMed]

133. Mizuno, N.; Misono, M. Heterogeneous Catalysis. *Chem. Rev.* **1998**, *98*, 199–218. [CrossRef] [PubMed]

134. Dong, C.; Li, Y.; Cheng, D.; Zhang, M.; Liu, J.; Wang, Y.-G.; Xiao, D.; Ma, D. Supported Metal Clusters: Fabrication and Application in Heterogeneous Catalysis. *ACS Catal.* **2020**, *10*, 11011–11045. [CrossRef]

135. Cuenya, B.R. Synthesis and catalytic properties of metal nanoparticles: Size, shape, support, composition, and oxidation state effects. *Thin Solid Film.* **2010**, *518*, 3127–3150. [CrossRef]

136. Tauster, S.J. Strong metal-support interactions. *Acc. Chem. Res.* **1987**, *20*, 389–394. [CrossRef]

137. Hansen, T.W.; DeLaRiva, A.T.; Challa, S.R.; Datye, A.K. Sintering of Catalytic Nanoparticles: Particle Migration or Ostwald Ripening? *Acc. Chem. Res.* **2013**, *46*, 1720–1730. [CrossRef]

138. Challa, S.R.; Delariva, A.T.; Hansen, T.W.; Helveg, S.; Sehested, J.; Hansen, P.L.; Garzon, F.; Datye, A.K. Relating Rates of Catalyst Sintering to the Disappearance of Individual Nanoparticles during Ostwald Ripening. *J. Am. Chem. Soc.* **2011**, *133*, 20672–20675. [CrossRef]

139. Yang, X.-Y.; Li, Z.-Q.; Liu, B.; Klein-Hofmann, A.; Tian, G.; Feng, Y.-F.; Ding, Y.; Su, D.S.; Xiao, F.-S. "Fish-in-Net" Encapsulation of Enzymes in Macroporous Cages for Stable, Reusable, and Active Heterogeneous Biocatalysts. *Adv. Mater.* **2006**, *18*, 410–414. [CrossRef]

140. Rungtaweevoranit, B.; Baek, J.; Araujo, J.R.; Archanjo, B.S.; Choi, K.M.; Yaghi, O.M.; Somorjai, G.A. Copper Nanocrystals Encapsulated in Zr-based Metal–Organic Frameworks for Highly Selective CO_2 Hydrogenation to Methanol. *Nano Lett.* **2016**, *16*, 7645–7649. [CrossRef]

141. Kobayashi, H.; Taylor, J.M.; Mitsuka, Y.; Ogiwara, N.; Yamamoto, T.; Toriyama, T.; Matsumura, S.; Kitagawa, H. Charge transfer dependence on CO_2 hydrogenation activity to methanol in Cu nanoparticles covered with metal–organic framework systems. *Chem. Sci.* **2019**, *10*, 3289–3294. [CrossRef]

142. Zhu, Y.; Zheng, J.; Ye, J.; Cui, Y.; Koh, K.; Kovarik, L.; Camaioni, D.M.; Fulton, J.L.; Truhlar, D.G.; Neurock, M.; et al. Copper-zirconia interfaces in UiO-66 enable selective catalytic hydrogenation of CO_2 to methanol. *Nat. Commun.* **2020**, *11*, 5849. [CrossRef]

143. Ye, J.; Neurock, M.; Truhlar, D.G. Effect of Missing-Linker Defects on CO_2 Hydrogenation to Methanol by Cu Nanoparticles in UiO-66. *J. Phys. Chem. C* **2022**, *126*, 13157–13167. [CrossRef]

144. Zheng, Z.; Xu, H.; Xu, Z.; Ge, J. A Monodispersed Spherical Zr-Based Metal–Organic Framework Catalyst, Pt/Au@ Pd@ UIO-66, Comprising an Au@ Pd Core–Shell Encapsulated in a UIO-66 Center and Its Highly Selective CO_2 Hydrogenation to Produce CO. *Small* **2018**, *14*, 1702812. [CrossRef] [PubMed]

145. An, B.; Zhang, J.; Cheng, K.; Ji, P.; Wang, C.; Lin, W. Confinement of Ultrasmall Cu/ZnOx Nanoparticles in Metal–Organic Frameworks for Selective Methanol Synthesis from Catalytic Hydrogenation of CO_2. *J. Am. Chem. Soc.* **2017**, *139*, 3834–3840. [CrossRef]

146. Yu, J.; Chen, G.; Guo, Q.; Guo, X.; Da Costa, P.; Mao, D. Ultrasmall bimetallic Cu/ZnOx nanoparticles encapsulated in UiO-66 by deposition–precipitation method for CO_2 hydrogenation to methanol. *Fuel* **2022**, *324*, 124694. [CrossRef]

147. Jiang, Q.; Lan, D.; Zhao, G.; Xu, H.; Gong, X.; Liu, J.; Shi, Y.; Zhang, L.; Fang, H.; Cheng, D. Converting CO_2 Hydrogenation Products from Paraffins to Olefins: Modification of Zeolite Surface Properties by a UIO-n Membrane. *ACS Catal.* **2022**, *12*, 5894–5902. [CrossRef]

148. Wu, Y.; Lan, D.; Liu, J.; Ge, J.; Xu, H.; Han, Y.; Zhang, H.; Pan, X.; Xu, Z.; Liu, J. UIO66-membranized SAPO-34 Pt catalyst for enhanced carbon dioxide conversion efficiency. *Mater. Today Energy* **2021**, *21*, 100781. [CrossRef]

149. Pan, X.; Xu, H.; Zhao, X.; Zhang, H. Metal–Organic Framework-Membranized Bicomponent Core–Shell Catalyst HZSM-5@UIO-66-NH$_2$/Pd for CO_2 Selective Conversion. *ACS Sustain. Chem. Eng.* **2020**, *8*, 1087–1094. [CrossRef]

150. Liao, F.; Wu, X.-P.; Zheng, J.; Li, M.M.-J.; Kroner, A.; Zeng, Z.; Hong, X.; Yuan, Y.; Gong, X.-Q.; Tsang, S.C.E. A promising low pressure methanol synthesis route from CO_2 hydrogenation over Pd@Zn core–shell catalysts. *Green Chem.* **2017**, *19*, 270–280. [CrossRef]

151. Bahruji, H.; Bowker, M.; Hutchings, G.; Dimitratos, N.; Wells, P.; Gibson, E.; Jones, W.; Brookes, C.; Morgan, D.; Lalev, G. Pd/ZnO catalysts for direct CO_2 hydrogenation to methanol. *J. Catal.* **2016**, *343*, 133–146. [CrossRef]

152. Férey, G.; Mellot-Draznieks, C.; Serre, C.; Millange, F.; Dutour, J.; Surblé, S.; Margiolaki, I. A chromium terephthalate-based solid with unusually large pore volumes and surface area. *Science* **2005**, *309*, 2040–2042. [CrossRef] [PubMed]

153. Howarth, A.J.; Liu, Y.; Li, P.; Li, Z.; Wang, T.C.; Hupp, J.T.; Farha, O.K. Chemical, thermal and mechanical stabilities of metal–organic frameworks. *Nat. Rev. Mater.* **2016**, *1*, 15018. [CrossRef]

154. Healy, C.; Patil, K.M.; Wilson, B.H.; Hermanspahn, L.; Harvey-Reid, N.C.; Howard, B.I.; Kleinjan, C.; Kolien, J.; Payet, F.; Telfer, S.G. The thermal stability of metal-organic frameworks. *Coord. Chem. Rev.* **2020**, *419*, 213388. [CrossRef]

155. Gascon, J.; Corma, A.; Kapteijn, F.; Llabres i Xamena, F.X. Metal organic framework catalysis: Quo vadis? *ACS Catal.* **2014**, *4*, 361–378. [CrossRef]

156. Yang, S.J.; Kim, T.; Im, J.H.; Kim, Y.S.; Lee, K.; Jung, H.; Park, C.R. MOF-Derived Hierarchically Porous Carbon with Exceptional Porosity and Hydrogen Storage Capacity. *Chem. Mater.* **2012**, *24*, 464–470. [CrossRef]

157. Lu, G.; Li, S.; Guo, Z.; Farha, O.K.; Hauser, B.G.; Qi, X.; Wang, Y.; Wang, X.; Han, S.; Liu, X.; et al. Imparting functionality to a metal–organic framework material by controlled nanoparticle encapsulation. *Nat. Chem.* **2012**, *4*, 310–316. [CrossRef]

158. Liu, B.; Shioyama, H.; Akita, T.; Xu, Q. Metal-Organic Framework as a Template for Porous Carbon Synthesis. *J. Am. Chem. Soc.* **2008**, *130*, 5390–5391. [CrossRef]

159. Lee, H.J.; Cho, W.; Lim, E.; Oh, M. One-pot synthesis of magnetic particle-embedded porous carbon composites from metal–organic frameworks and their sorption properties. *Chem. Commun.* **2014**, *50*, 5476–5479. [CrossRef]

160. Zhang, H.; Wang, T.; Wang, J.; Liu, H.; Dao, T.D.; Li, M.; Liu, G.; Meng, X.; Chang, K.; Shi, L. Surface-plasmon-enhanced photodriven CO_2 reduction catalyzed by metal–organic-framework-derived iron nanoparticles encapsulated by ultrathin carbon layers. *Adv. Mater.* **2016**, *28*, 3703–3710. [CrossRef]

161. Lu, X.; Liu, Y.; He, Y.; Kuhn, A.N.; Shih, P.-C.; Sun, C.-J.; Wen, X.; Shi, C.; Yang, H. Cobalt-Based Nonprecious Metal Catalysts Derived from Metal–Organic Frameworks for High-Rate Hydrogenation of Carbon Dioxide. *ACS Appl. Mater. Inter.* **2019**, *11*, 27717–27726. [CrossRef] [PubMed]

162. Yang, Y.; Jia, L.; Hou, B.; Li, D.; Wang, J.; Sun, Y. The Correlation of Interfacial Interaction and Catalytic Performance of N-Doped Mesoporous Carbon Supported Cobalt Nanoparticles for Fischer–Tropsch Synthesis. *J. Phys. Chem. C* **2014**, *118*, 268–277. [CrossRef]

163. Yang, Y.; Jia, L.; Hou, B.; Li, D.; Wang, J.; Sun, Y. The Effect of Nitrogen on the Autoreduction of Cobalt Nanoparticles Supported on Nitrogen-Doped Ordered Mesoporous Carbon for the Fischer–Tropsch Synthesis. *ChemCatChem* **2014**, *6*, 319–327. [CrossRef]

164. Kattel, S.; Ramírez, P.J.; Chen, J.G.; Rodriguez, J.A.; Liu, P. Active sites for CO_2 hydrogenation to methanol on Cu/ZnO catalysts. *Science* **2017**, *355*, 1296–1299. [CrossRef] [PubMed]

165. Dietz, L.; Piccinin, S.; Maestri, M. Mechanistic Insights into CO_2 Activation via Reverse Water–Gas Shift on Metal Surfaces. *J. Phys. Chem. C* **2015**, *119*, 4959–4966. [CrossRef]

166. Chen, C.-S.; Cheng, W.-H.; Lin, S.-S. Mechanism of CO formation in reverse water–gas shift reaction over Cu/Al_2O_3 catalyst. *Catal. Lett.* **2000**, *68*, 45–48. [CrossRef]

167. Qiu, B.; Yang, C.; Guo, W.; Xu, Y.; Liang, Z.; Ma, D.; Zou, R. Highly dispersed Co-based Fischer–Tropsch synthesis catalysts from metal–organic frameworks. *J. Mater. Chem. A* **2017**, *5*, 8081–8086. [CrossRef]

168. Lin, X.; Wang, S.; Tu, W.; Hu, Z.; Ding, Z.; Hou, Y.; Xu, R.; Dai, W. MOF-derived hierarchical hollow spheres composed of carbon-confined Ni nanoparticles for efficient CO2 methanation. *Catal. Sci. Technol.* **2019**, *9*, 731–738. [CrossRef]

169. Liu, J.; Zhang, A.; Liu, M.; Hu, S.; Ding, F.; Song, C.; Guo, X. Fe-MOF-derived highly active catalysts for carbon dioxide hydrogenation to valuable hydrocarbons. *J. CO2 Util.* **2017**, *21*, 100–107. [CrossRef]

170. Visconti, C.G.; Martinelli, M.; Falbo, L.; Infantes-Molina, A.; Lietti, L.; Forzatti, P.; Iaquaniello, G.; Palo, E.; Picutti, B.; Brignoli, F. CO_2 hydrogenation to lower olefins on a high surface area K-promoted bulk Fe-catalyst. *Appl. Catal. B Environ.* **2017**, *200*, 530–542. [CrossRef]

171. Al-Dossary, M.; Ismail, A.A.; Fierro, J.L.G.; Bouzid, H.; Al-Sayari, S.A. Effect of Mn loading onto MnFeO nanocomposites for the CO_2 hydrogenation reaction. *Appl. Catal. B Environ.* **2015**, *165*, 651–660. [CrossRef]

172. Herranz, T.; Rojas, S.; Pérez-Alonso, F.J.; Ojeda, M.; Terreros, P.; Fierro, J.L.G. Hydrogenation of carbon oxides over promoted Fe-Mn catalysts prepared by the microemulsion methodology. *Appl. Catal. A Gen.* **2006**, *311*, 66–75. [CrossRef]

173. Niemelä, M.; Nokkosmäki, M. Activation of carbon dioxide on Fe-catalysts. *Catal. Today* **2005**, *100*, 269–274. [CrossRef]

174. Liu, J.; Sun, Y.; Jiang, X.; Zhang, A.; Song, C.; Guo, X. Pyrolyzing ZIF-8 to N-doped porous carbon facilitated by iron and potassium for CO_2 hydrogenation to value-added hydrocarbons. *J. CO2 Util.* **2018**, *25*, 120–127. [CrossRef]

175. Whittaker, T.; Kumar, K.B.S.; Peterson, C.; Pollock, M.N.; Grabow, L.C.; Chandler, B.D. H_2 Oxidation over Supported Au Nanoparticle Catalysts: Evidence for Heterolytic H2 Activation at the Metal–Support Interface. *J. Am. Chem. Soc.* **2018**, *140*, 16469–16487. [CrossRef]

176. Peng, L.; Zheng, X.; Li, L.; Zhang, L.; Yang, N.; Xiong, K.; Chen, H.; Li, J.; Wei, Z. Chimney effect of the interface in metal oxide/metal composite catalysts on the hydrogen evolution reaction. *Appl. Catal. B Environ.* **2019**, *245*, 122–129. [CrossRef]

177. Yang, X.; Yu, X.; Lin, M.; Ge, M.; Zhao, Y.; Wang, F. Interface effect of mixed phase Pt/ZrO_2 catalysts for HCHO oxidation at ambient temperature. *J. Mater. Chem. A* **2017**, *5*, 13799–13806. [CrossRef]

178. Yang, X.; Kattel, S.; Senanayake, S.D.; Boscoboinik, J.A.; Nie, X.; Graciani, J.; Rodriguez, J.A.; Liu, P.; Stacchiola, D.J.; Chen, J.G. Low Pressure CO_2 Hydrogenation to Methanol over Gold Nanoparticles Activated on a CeO_x/TiO_2 Interface. *J. Am. Chem. Soc.* **2015**, *137*, 10104–10107. [CrossRef] [PubMed]

179. Lam, E.; Corral-Pérez, J.J.; Larmier, K.; Noh, G.; Wolf, P.; Comas-Vives, A.; Urakawa, A.; Copéret, C. CO_2 Hydrogenation on Cu/Al_2O_3: Role of the Metal/Support Interface in Driving Activity and Selectivity of a Bifunctional Catalyst. *Angew. Chem. Int. Ed.* **2019**, *58*, 13989–13996. [CrossRef] [PubMed]

180. Ali, K.A.; Abdullah, A.Z.; Mohamed, A.R. Recent development in catalytic technologies for methanol synthesis from renewable sources: A critical review. *Renew. Sustain. Energy Rev.* **2015**, *44*, 508–518. [CrossRef]

181. Martin, O.; Pérez-Ramírez, J. New and revisited insights into the promotion of methanol synthesis catalysts by CO_2. *Catal. Sci. Technol.* **2013**, *3*, 3343–3352. [CrossRef]

182. Arena, F.; Barbera, K.; Italiano, G.; Bonura, G.; Spadaro, L.; Frusteri, F. Synthesis, characterization and activity pattern of $Cu–ZnO/ZrO_2$ catalysts in the hydrogenation of carbon dioxide to methanol. *J. Catal.* **2007**, *249*, 185–194. [CrossRef]

183. Porosoff, M.D.; Yan, B.; Chen, J.G. Catalytic reduction of CO_2 by H_2 for synthesis of CO, methanol and hydrocarbons: Challenges and opportunities. *Energy Environ. Sci.* **2016**, *9*, 62–73. [CrossRef]

184. Bansode, A.; Urakawa, A. Towards full one-pass conversion of carbon dioxide to methanol and methanol-derived products. *J. Catal.* **2014**, *309*, 66–70. [CrossRef]

185. Le Valant, A.; Comminges, C.; Tisseraud, C.; Canaff, C.; Pinard, L.; Pouilloux, Y. The Cu–ZnO synergy in methanol synthesis from CO_2, Part 1: Origin of active site explained by experimental studies and a sphere contact quantification model on Cu+ZnO mechanical mixtures. *J. Catal.* **2015**, *324*, 41–49. [CrossRef]

186. Bansode, A.; Tidona, B.; von Rohr, P.R.; Urakawa, A. Impact of K and Ba promoters on CO2 hydrogenation over Cu/Al_2O_3 catalysts at high pressure. *Catal. Sci. Technol.* **2013**, *3*, 767–778. [CrossRef]

187. Gao, P.; Li, F.; Zhao, N.; Xiao, F.; Wei, W.; Zhong, L.; Sun, Y. Influence of modifier (Mn, La, Ce, Zr and Y) on the performance of Cu/Zn/Al catalysts via hydrotalcite-like precursors for CO_2 hydrogenation to methanol. *Appl. Catal. A Gen.* **2013**, *468*, 442–452. [CrossRef]

188. Bavykina, A.; Yarulina, I.; Al Abdulghani, A.J.; Gevers, L.; Hedhili, M.N.; Miao, X.; Galilea, A.R.; Pustovarenko, A.; Dikhtiarenko, A.; Cadiau, A.; et al. Turning a Methanation Co Catalyst into an In–Co Methanol Producer. *ACS Catal.* **2019**, *9*, 6910–6918. [CrossRef]

189. Frei, M.S.; Mondelli, C.; García-Muelas, R.; Kley, K.S.; Puértolas, B.; López, N.; Safonova, O.V.; Stewart, J.A.; Curulla Ferré, D.; Pérez-Ramírez, J. Atomic-scale engineering of indium oxide promotion by palladium for methanol production via CO_2 hydrogenation. *Nat. Commun.* **2019**, *10*, 3377. [CrossRef]

190. Martin, O.; Martín, A.J.; Mondelli, C.; Mitchell, S.; Segawa, T.F.; Hauert, R.; Drouilly, C.; Curulla-Ferré, D.; Pérez-Ramírez, J. Indium Oxide as a Superior Catalyst for Methanol Synthesis by CO_2 Hydrogenation. *Angew. Chem. Int. Ed.* **2016**, *55*, 6261–6265. [CrossRef]

191. Pustovarenko, A.; Dikhtiarenko, A.; Bavykina, A.; Gevers, L.; Ramírez, A.; Russkikh, A.; Telalovic, S.; Aguilar, A.; Hazemann, J.-L.; Ould-Chikh, S.; et al. Metal–Organic Framework-Derived Synthesis of Cobalt Indium Catalysts for the Hydrogenation of CO_2 to Methanol. *ACS Catal.* **2020**, *10*, 5064–5076. [CrossRef]

192. Zhang, C.; Liao, P.; Wang, H.; Sun, J.; Gao, P. Preparation of novel bimetallic CuZn-BTC coordination polymer nanorod for methanol synthesis from CO_2 hydrogenation. *Mater. Chem. Phys.* **2018**, *215*, 211–220. [CrossRef]

193. Zuo, Z.-J.; Li, N.; Liu, S.-Z.; Han, P.-D.; Huang, W. Initial stages of oxidation for Cu-based catalysts using density functional theory. *Appl. Surf. Sci.* **2016**, *366*, 85–94. [CrossRef]

194. Fan, X.; Tang, Q.-L.; Zhang, X.; Zhang, T.-T.; Wang, Q.; Duan, X.-X.; Zhang, M.-L.; Yao, M.-Y. Comprehensive theoretical analysis of the influence of surface alloying by zinc on the catalytic performance of Cu(110) for the production of methanol from CO_2 selective hydrogenation: Part 1—Thermochemical aspects. *Appl. Surf. Sci.* **2019**, *469*, 841–853. [CrossRef]

195. Behrens, M.; Zander, S.; Kurr, P.; Jacobsen, N.; Senker, J.; Koch, G.; Ressler, T.; Fischer, R.W.; Schlögl, R. Performance Improvement of Nanocatalysts by Promoter-Induced Defects in the Support Material: Methanol Synthesis over Cu/ZnO:Al. *J. Am. Chem. Soc.* **2013**, *135*, 6061–6068. [CrossRef]

196. Murthy, P.S.; Liang, W.; Jiang, Y.; Huang, J. Cu-Based Nanocatalysts for CO_2 Hydrogenation to Methanol. *Energy Fuels* **2021**, *35*, 8558–8584. [CrossRef]

197. Chen, G.; Yu, J.; Li, G.; Zheng, X.; Mao, H.; Mao, D. Cu^+-ZrO_2 interfacial sites with highly dispersed copper nanoparticles derived from Cu@UiO-67 hybrid for efficient CO_2 hydrogenation to methanol. *Int. J. Hydrog. Energy* **2022**, *48*, 2605–2616. [CrossRef]

198. Yu, J.; Liu, S.; Mu, X.; Yang, G.; Luo, X.; Lester, E.; Wu, T. Cu-ZrO_2 catalysts with highly dispersed Cu nanoclusters derived from ZrO_2@ HKUST-1 composites for the enhanced CO_2 hydrogenation to methanol. *Chem. Eng. J.* **2021**, *419*, 129656. [CrossRef]

199. Yin, Y.; Hu, B.; Li, X.; Zhou, X.; Hong, X.; Liu, G. Pd@zeolitic imidazolate framework-8 derived PdZn alloy catalysts for efficient hydrogenation of CO_2 to methanol. *Appl. Catal. B Environ.* **2018**, *234*, 143–152. [CrossRef]

200. Cai, Z.; Dai, J.; Li, W.; Tan, K.B.; Huang, Z.; Zhan, G.; Huang, J.; Li, Q. Pd Supported on MIL-68(In)-Derived In_2O_3 Nanotubes as Superior Catalysts to Boost CO_2 Hydrogenation to Methanol. *ACS Catal.* **2020**, *10*, 13275–13289. [CrossRef]

201. Lu, X.; Wang, H.; Yang, Y.; Wang, Z. Microstructural manipulation of MFI-type zeolite films/membranes: Current status and perspectives. *J. Membr. Sci* **2022**, *662*, 120931. [CrossRef]